

# A generalized Townsend's theory for Paschen curves in planar, cylindrical, and spherical geometries in planetary atmospheres

Jeremy A Riouset<sup>1</sup>, Joshua Mendez Harper<sup>2</sup>, Josef Dufek<sup>2</sup>, Jared P Nelson<sup>1</sup>, and Annelisa B Esparza<sup>3</sup>

<sup>1</sup>Embry-Riddle Aeronautical University

<sup>2</sup>University of Oregon

<sup>3</sup>Florida Institute of Technology

December 31, 2022

## Abstract

In this work, we focus on plasma discharges produced between two electrodes with a high potential difference, resulting in the ionization of the neutral particles supporting a current in the gaseous medium. At low currents and low temperatures, this process can create luminescent emissions: the glow and corona discharges. The parallel plate geometry used in Townsend's (1900) theory lets us develop a theoretical formalism, with explicit solutions for the critical voltage effectively reproducing experimental Paschen curves. However, most discharge processes occur in non-parallel plate geometries, such as discharges between grains or ice particles in multiphase flows. Here, we propose a generalization of the classic parallel plate configurations to concentric spherical and coaxial cylindrical geometries in Earth, Mars, Titan, and Venus atmospheres. In a spherical case, a small radius effectively represents a sharp tip rod, while larger, centimeter-scale radii represent blunted tips. Similarly, in a cylindrical case, a small radius corresponds to a thin wire. We solve continuity equations in the gap and estimate a critical radius and minimum breakdown voltage that allows ionization of neutral gas and formation of a glow discharge. We show that glow coronæ form more easily in Mars's low-pressure, CO<sub>2</sub>-rich atmosphere than in Earth's high-pressure atmosphere. Additionally, we present breakdown criteria for Titan and Venus. We further demonstrate that critical voltage minima occur at 0.5 cm·Torr for all three investigated geometries, suggesting easier initiation around millimeter-size particles in dust and water clouds and could be readily extended to examine other multiphase flows with inertial particles.

1 **A generalized Townsend's theory for Paschen curves in**  
2 **planar, cylindrical, and spherical geometries in**  
3 **planetary atmospheres**

4 **Jeremy A. Rioussset<sup>1,2</sup>, Joshua S. Méndez Harper<sup>3</sup>, Josef Dufek<sup>3</sup>, Jared P.**  
5 **Nelson<sup>2</sup>, Annelisa B. Esparza<sup>2</sup>**

6 <sup>1</sup>Aerospace, Physics & Space Sciences Department, Florida Institute of Technology, 150 W Univ. Blvd.,  
7 Melbourne, FL, 32901, USA

8 <sup>2</sup>Department of Physical Sciences, Space and Atmospheric Instrumentation Lab, Embry-Riddle  
9 Aeronautical University, 1 Aerospace Blvd., Daytona Beach, FL, 32114, USA

10 <sup>3</sup>Department of Earth Sciences, University of Oregon, 1272 University of Oregon, Eugene, OR, 97403,  
11 USA

12 **Key Points:**

- 13 • Numerical modeling lets us study glow coronas around spherical and cylindrical  
14 electrodes based on Paschen theory.
- 15 • Critical voltages are found at  $pd$  and  $pa \approx 0.5 \text{ cm} \cdot \text{Torr}$ , suggesting easier initiation  
16 around mm-size particles in dust and water clouds.
- 17 • Glow corona formation is easier in Mars's low pressure, CO<sub>2</sub>-rich atmosphere than  
18 in Earth's high-pressure atmosphere.

---

Corresponding author: Jeremy A. Rioussset, [rioussjej@erau.edu](mailto:rioussjej@erau.edu)

19 **Abstract**

20 In this work, we focus on plasma discharges produced between two electrodes with a high  
 21 potential difference, resulting in the ionization of the neutral particles supporting a cur-  
 22 rent in the gaseous medium. At low currents and low temperatures, this process can cre-  
 23 ate luminescent emissions: the glow and corona discharges. The parallel plate geometry  
 24 used in Townsend’s (1900) theory lets us develop a theoretical formalism, with explicit  
 25 solutions for the critical voltage effectively reproducing experimental Paschen curves. How-  
 26 ever, most discharge processes occur in non-parallel plate geometries, such as discharges  
 27 between grains or ice particles in multiphase flows. Here, we propose a generalization  
 28 of the classic parallel plate configurations to concentric spherical and coaxial cylindri-  
 29 cal geometries in Earth, Mars, Titan, and Venus atmospheres. In a spherical case, a small  
 30 radius effectively represents a sharp tip rod, while larger, centimeter-scale radii repre-  
 31 sent blunted tips. Similarly, in a cylindrical case, a small radius corresponds to a thin  
 32 wire. We solve continuity equations in the gap and estimate a critical radius and min-  
 33 imum breakdown voltage that allows ionization of neutral gas and formation of a glow  
 34 discharge. We show that glow coronæ form more easily in Mars’s low-pressure, CO<sub>2</sub>-rich  
 35 atmosphere than in Earth’s high-pressure atmosphere. Additionally, we present break-  
 36 down criteria for Titan and Venus. We further demonstrate that critical voltage minima  
 37 occur at 0.5 cm·Torr for all three investigated geometries, suggesting easier initiation around  
 38 millimeter-size particles in dust and water clouds and could be readily extended to ex-  
 39 amine other multiphase flows with inertial particles.

40 **Plain Language Summary**

41 In this work, we focus on plasma discharges between two electrodes with a high volt-  
 42 age difference. The result is a conversion of the medium from a dielectric to a conduc-  
 43 tor. At low currents and low temperatures, this process can create luminescent emissions:  
 44 the so-called glow and corona discharges. We extend the parallel plate geometry devel-  
 45 oped in Townsend’s (1900) classical theory to determine the critical discharge voltages  
 46 of spheres and cylinders more likely to be encountered as particles in an atmosphere. Here,  
 47 we propose a generalization of the classic parallel plate configurations to concentric spheres  
 48 and coaxial cylinders in Earth, Mars, Venus, and Titan atmospheres. We computation-  
 49 ally solve the continuity equations in the gap between objects and ultimately calculate  
 50 critical electric fields for self-sustained discharges. We show that glow coronæ form more

51 easily in Mars’s low-pressure, CO<sub>2</sub>-rich atmosphere than in Earth’s high-pressure atmo-  
52 sphere. Additionally, we present breakdown criteria for Titan and Venus. We further demon-  
53 strate that critical voltage minima occur near 0.5 cm · Torr for all three investigated ge-  
54 ometries, suggesting easier initiation around millimeter-size particles in dust and water  
55 clouds.

## 56 1 Introduction

57 The recent and planned *in-situ* exploration of planetary bodies in the solar system  
58 motivates a better understanding of electrostatic hazards under conditions relevant to  
59 each object. Specifically, the potential for discharge involves a complex interplay between  
60 atmospheric pressure variation, gas composition, realistic geometries of charged surfaces,  
61 and the presence of suspended solids in the atmosphere. The near-surface, diffuse con-  
62 ditions on present-day Mars may, in particular, present hazards associated with electro-  
63 static discharges for both robotic endeavors and potential crewed missions (Yair, 2012).  
64 Furthermore, the presence (or absence) of electrical discharges could have important im-  
65 plications for atmospheric chemistry and habitability (Tennakone, 2016; Hess et al., 2021).  
66 Any dielectric breakdown starts when the ambient electric field  $E$  exceeds a threshold  
67  $E_{\text{th}}$  (e.g., Raizer, 1991, p. 128), which depends on the nature of the discharge (e.g., leader,  
68 streamer, or glow) and its polarity (see e.g., Pasko, 2006, Figure 1 for discharge in air).  
69 Putative and confirmed extraterrestrial electrical discharges have been the topic of sev-  
70 eral studies (see reviews by Leblanc et al., 2008; Rioussset et al., 2020, and references therein).  
71 While most investigations have focused on lightning as a “transient, high-current elec-  
72 trical discharge whose path length is measured in kilometers” (Uman, 2001, p. 8 & Ta-  
73 ble 14.1), a noteworthy few have also investigated Transient Luminous Events, TLEs (e.g.,  
74 Bering et al., 2004; Dubrovin et al., 2010; Yair, 2012) and small-scale spark or glow dis-  
75 charges (e.g., Méndez Harper et al., 2018; Méndez Harper et al., 2021). Elucidating dis-  
76 charge criteria on extraterrestrial environments is complicated by a profound dearth of  
77 *in-situ* observational data. In the context of Mars, for example, the unfortunate fate of  
78 ExoMars’ Schiaparelli module (Déprez et al., 2014) prevented the first direct measure-  
79 ments of the electric field at the surface of the planet. Insight into the atmospheric elec-  
80 trical environment on Venus and Titan, the two other rocky worlds in our solar systems  
81 with atmospheres thick enough to support gas breakdown, is also scant. Consequently,

82 indirect measurements and analogies remain the only ways to gain insight into breakdown  
83 processes in planetary atmospheres.

84 The diverse span of atmospheric conditions on worlds in our own solar system sug-  
85 gests that the criteria that lead to breakdown in extraterrestrial environments may be  
86 equally disparate. Although both Mars and Venus host CO<sub>2</sub>-rich atmospheres, Venus  
87 maintains a near-surface atmospheric pressure  $\sim 10^4$  times higher than the Martian  
88 one (Zasova et al., 2007; Jakosky, Grebowsky, et al., 2015; Jakosky, Lin, et al., 2015; Sánchez-  
89 Lavega et al., 2017). On Titan, the atmospheric surface pressure is only slightly higher  
90 than Earth’s. However, Titan’s atmosphere is 4 times denser than Earth’s and signifi-  
91 cantly colder (90 K for Titan v. 287 K for Earth (Hörst, 2017)). Important chemical dif-  
92 ferences between worlds exist, too. Methane, for instance, is an important constituent  
93 of Titan’s nitrogen-rich atmosphere. Oxygen, while abundant in Earth’s atmosphere, ex-  
94 ists in trace amounts or is absent in the atmospheres of the other three worlds. Likewise  
95 there is significant variability in the composition, abundance, and presence of particu-  
96 lates in these atmospheres (e.g. silicate dust, ice, hydrocarbons), and multiphase topolo-  
97 gies may also be important for local discharge events. Using this diversity of atmospheric  
98 conditions (summarized in Table 1), we revisit Townsend’s (1900) seminal model for self-  
99 sustained dielectrical breakdown between parallel electrodes. Townsend developed the  
100 theory supporting what is now known as Paschen’s (1889) law. Paschen’s law states that  
101 the breakdown voltage between two electrodes is a function of the product of the pres-  
102 sure,  $p$ , and interelectrode distance,  $d$ . Townsend (1900) proved that this scaling law comes  
103 from the exponential increase of electron number density via avalanche multiplication  
104 and secondary ionization (e.g., Bazelyan & Raizer, 1998, pp. 31–32). Interestingly, these  
105 early studies already involved experiments in air, carbon dioxide, and hydrogen. These  
106 gases contribute significantly to many planetary atmospheres in our solar system, demon-  
107 strating that discharge processes are highly dependent on gas composition.

108 The elegance of Townsend’s theory rests in its simplicity and the sole requirement  
109 of an exponential approximation for the effective ionization coefficient  $\alpha$ . We revisit Townsend’s  
110 theory from first principles in Section 2. Townsend’s theory, however, assumes that the  
111 discharge occurs between two infinite parallel plates (i.e., a 1-D Cartesian geometry). To  
112 approach this configuration, experimental setups have adopted large flat electrodes with  
113 large radii  $R$ , and small gap size,  $d$ , so that  $R \gg d$  (e.g., Raizer (1991, p. 53); Lowke  
114 and D’Alessandro (2003); Stumbo (2013)). While such configurations are suitable for lab-

115 oratory experiments, they may not be representative of real discharge processes that in-  
 116 variably deal with complex geometries. In fact, natural electrical discharge events are  
 117 almost always associated with multiphase flows. For instance, discharges on Mars may  
 118 occur between small sand grains. Similarly, arcing could occur between two voltage-carrying  
 119 conductors under appropriate pressure-distance products. Thus, in the remainder of Sec-  
 120 tion 2, we demonstrate that an extension to cylindrical and spherical geometries is pos-  
 121 sible for Townsend’s theory provided one approximates the mobility  $\mu$ . We further de-  
 122 velop a generalized Townsend’s criterion for the ignition of self-sustained gas discharges

	Earth	Mars	Titan	Venus	
Molar fraction	Ar	$9.05 \times 10^{-3}$	$1.60 \times 10^{-2}$	$2.4 \times 10^{-2}$	–
	CH <sub>4</sub>	–	–	$2.7 \times 10^{-2}$	–
	CO	$1.84 \times 10^{-7}$	–	–	–
	CO <sub>2</sub>	$3.79 \times 10^{-3}$	$95.7 \times 10^{-2}$	–	$96.2 \times 10^{-2}$
	He	$5.04 \times 10^{-6}$	–	–	–
	N <sub>2</sub>	$75.68 \times 10^{-2}$	$2.7 \times 10^{-2}$	$94.9 \times 10^{-2}$	$3.5 \times 10^{-2}$
	N <sub>2</sub> O	$3.43 \times 10^{-7}$	–	–	–
	O <sub>2</sub>	$20.30 \times 10^{-2}$	–	–	–
	O <sub>3</sub>	$3.01 \times 10^{-8}$	–	–	–
$T$ (K)	273.04	231.2	93.9	737	
$N$ (m <sup>-3</sup> )	$2.688 \times 10^{25}$	$1.889 \times 10^{23}$	$1.150 \times 10^{26}$	$9.131 \times 10^{26}$	
Coeff.	$A$ (10 <sup>-20</sup> m <sup>2</sup> )	1.04	2.11	2.14	1.42
	$B$ (Td <sup>-1</sup> )	596.8	594.3	602.5	723.4
	$C$ (10 <sup>24</sup> /(Vms))	3.35	12.32	12.38	3.75
	$D$	-0.23	-0.46	-0.46	-0.23

**Table 1.** Input parameters for BOLSIG runs. Atmospheric parameters are from NASA’s Global Reference Atmospheric Models (GRAMs; EarthGRAM by Leslie (2008), MarsGRAM by H. L. Justh et al. (2010), TitanGRAM by H. Justh and Hoffman (2020), and VenusGRAM by H. L. Justh and Dwyer Cianciolo (2021)) taken at the surface  $z=0$  km on January 1<sup>st</sup>, 2000, 1200 UT, at 0° latitude and 0° longitude. These are the same surface conditions as in (Riousset et al., 2020). The coefficients  $A$ ,  $B$ ,  $C$ , and  $D$  define  $\tilde{a}/N$  and  $\tilde{\mu} \times N$  in (7).

123 for coaxial cylinders and concentric spheres. We show that the numerical solutions of  
 124 these equations yield the critical potential  $V_{\text{cr}}$  and corresponding electric field  $E_{\text{cr}}$  and  
 125 satisfy the same similarity laws as first introduced by Paschen (1889). Sections 3 and 4  
 126 will respectively discuss the results and implications of the new formalism, while section 5  
 127 will summarize the principal contributions of this paper.

## 128 **2 Model Formulation**

129 This section describes the model used to develop a criterion for the initiation of self-  
 130 sustained glow discharge between two one-dimensional electrodes located at  $r=a$  and  $b$ ,  
 131 where  $r$  is a coordinate along the direction normal to the surface of the electrode (Fig-  
 132 ure 1).

133 In the absence of free electric charges, Gauss's law for electric field  $\vec{E}$  reduces to  
 134  $\nabla \cdot \vec{E} = 0$ . It further simplifies into:

$$135 \frac{1}{r^\delta} \frac{dr^\delta E(r)}{dr} = 0, \quad (1)$$

136 where  $\delta = 0, 1,$  and  $2$  for the Cartesian, cylindrical, spherical 1-D geometries displayed  
 137 in Figures 1a, 1b, and 1c, respectively. If *space charges do not contribute significantly*  
 138 *to the total electric field between the electrodes*, then:  
 139

$$140 E(r) = E_a \left( \frac{a}{r} \right)^\delta, \quad (2)$$

141 with  $E_a = E(a)$  and  $a \leq r \leq b$ .

142 The ignition of an electron avalanche between two electrodes depends on the effec-  
 143 tive ionization frequency  $\nu_i$  and the poorly understood secondary ionization coefficient  
 144  $\gamma$  (Raizer, 1991, p. 74). Townsend's effective ionization coefficient  $\alpha$  provides a conve-  
 145 nient description of the primary ionization per unit length:  
 146

$$147 \alpha = \frac{\nu_i}{\|\vec{u}\|} = \frac{\nu_i}{u} \quad (3)$$

148 where the drift velocity  $\vec{u}$  depends on the mobility  $\mu$  as follows (e.g., Chen, 1984, p. 66):

$$150 \vec{u} = \mu(E) \vec{E}. \quad (4)$$

151 Thus,  $\alpha$  depends on  $E$  as follows:

$$152 \alpha(E) = \frac{\nu_i(E)}{\mu(E)E} \quad (5)$$

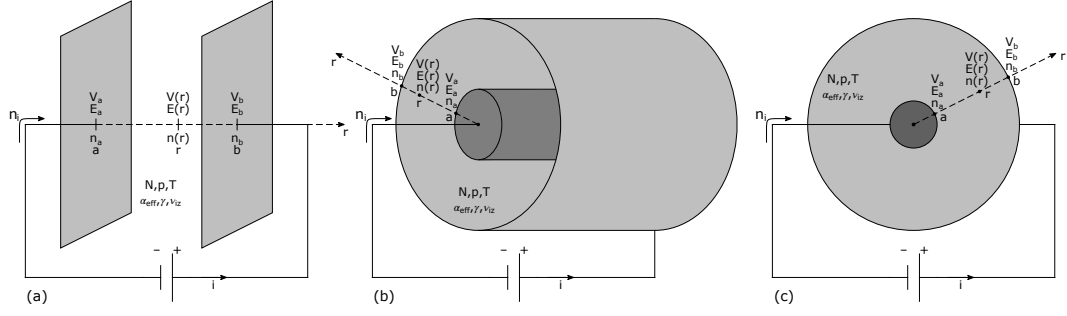


**Figure 1.** Townsend's discharge in one-dimensional geometries: (a) Parallel plates (Cartesian); (b) Coaxial cylindrical electrodes; (c) Concentric spherical electrodes. The gas in between the electrodes has the number density  $N$  ( $\text{m}^{-3}$ ) at the temperature  $T$  (K) under the pressure  $p$  (Pa). The avalanche is characterized by Townsend's effective ionization coefficient  $\alpha$  ( $\text{m}^{-1}$ ), the secondary ionization coefficient  $\gamma$ , and effective ionization frequency  $\nu_i$  ( $\text{s}^{-1}$ ). The quantities  $n_i$ ,  $n_a$ ,  $n(r)$ , and  $n_b$  correspond to the electron density in  $\text{m}^{-3}$  carried by the electronic current  $i$ , emitted from the cathode at  $a$ , measured at  $r$ , and received at the anode at  $b$ , respectively ( $a \leq r \leq b$ ). The corresponding electric potential and field are denoted  $V$  (V) and  $E$  (V/m).

154 Townsend's theory provides an analytical solution to Paschen curves if  $\alpha$  approximately  
 155 fits an exponential function:

$$156 \quad \tilde{\alpha} = Ap \exp(-Bp/E), \quad (6)$$

157  
 158 where  $p$  is the neutral gas pressure (e.g., Raizer, 1991, pp. 149). Experimental studies  
 159 typically adopt pressure-based scaling with  $p$  in Torr and  $\alpha$  in  $\text{cm}^{-1}$  (e.g., Raizer, 1991,  
 160 pp. 133) giving  $\alpha/p$  in  $1/(\text{cm} \cdot \text{Torr})$ . On the other hand, theoretical investigations usu-  
 161 ally prefer density-based scaling with  $N$ , the neutral gas number density in  $\text{m}^{-3}$  and  $\alpha$   
 162 in  $\text{m}^{-1}$ , returning  $\alpha/N$  in  $\text{m}^2$  (e.g., Hagelaar, 2015; Lieberman & Lichtenberg, 2005, p. 545).  
 163 Both formulations are equivalent, provided that the system remains approximately at  
 164 the temperature  $T$  and that the gas obeys the ideal gas law, namely  $p = Nk_B T$ , where  
 165  $k_B$  is the Boltzmann constant. Consequently, we can write:

$$166 \quad \frac{\tilde{\alpha}}{N} = A \exp\left(-\frac{B}{E/N}\right) \quad (7a)$$

$$167 \quad \tilde{\mu} \times N = C \left(\frac{E}{N}\right)^D \quad (7b)$$

168  
 169  
 170

171 where  $A$ ,  $B$ ,  $C$ , and  $D$  are the coefficients from a fit to the reduced Townsend's effective  
 172 ionization  $\alpha/N$  and mobility  $\mu \times N$  (Figure 2) for the atmospheres considered here  
 173 (Table 1).

174 The condition for self-sustainability of Townsend's discharges in any of the geome-  
 175 tries shown in Figure 1 starts with the continuity equation:

$$176 \quad \frac{\partial n}{\partial t} + \nabla \cdot n\vec{u} = n\nu_1 \quad (8)$$

178 where  $n$  is the plasma density.

179 Combining Equations (1), (3), and (8) in a steady state ( $\partial/\partial t = 0$ ) yields  $\frac{1}{r^\delta} \frac{d}{dr} (r^\delta n u) =$   
 180  $n\alpha u$ . Using Equation (4), this simplifies further into:

$$181 \quad \frac{d \ln(r^\delta n \mu(E) E)}{dr} = \alpha(E). \quad (9)$$

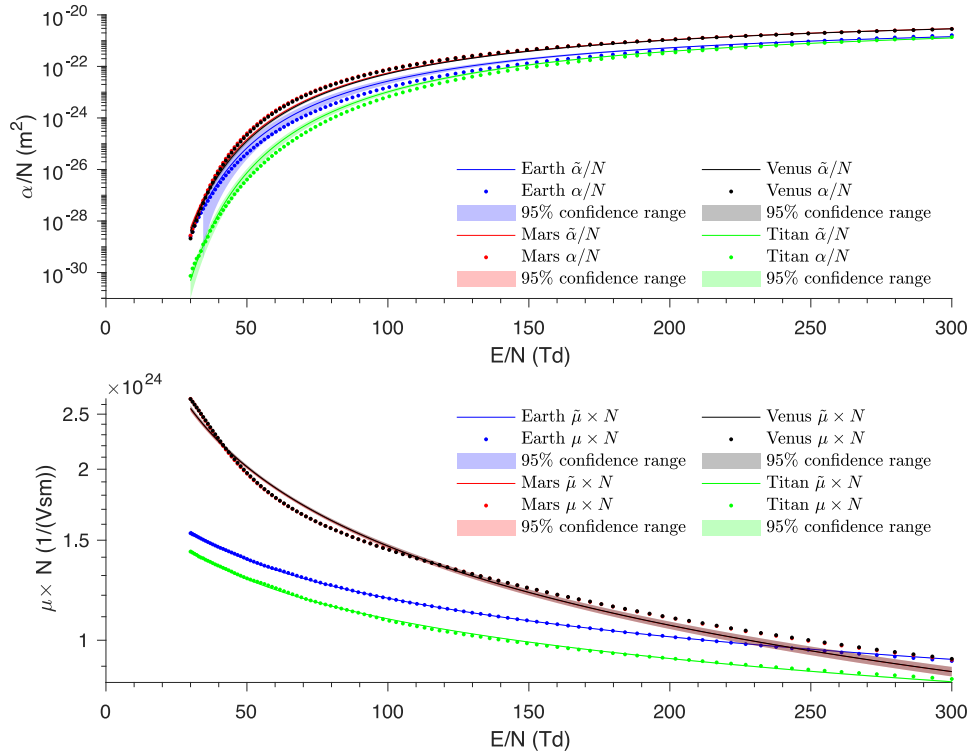


**Figure 2.** Scaling laws for (a) the reduced effective Townsend's ionization coefficient  $\alpha/N$  and (b) reduced mobility  $\mu \times N$  plotted against the reduced electric field  $E/N$ . Blue, red, gray, and green colors correspond to Earth-, Mars-, Venus-, and Titan-like atmospheres, respectively (see Table 1).

183 From Equation (2), we have  $E_a a^\delta = E_b b^\delta$ . If  $A_{\text{av}} = n_b/n_a$  is the avalanche coefficient  
 184 defined as the ratio of the number densities  $n_a = n(a)$  and  $n_b = n(b)$ , then Equa-  
 185 tion (9) yields:

$$186 \quad A_{\text{av}} = \frac{n_b}{n_a} = \frac{\mu(E_a)}{\mu(E_b)} \exp\left(\int_a^b \alpha(E) dr\right) \quad (10)$$

## 188 2.1 Sustainability

189 Call  $n_i$  the number density of charges from the electronic current  $i$  and  $n_\gamma$  the one  
 190 from secondary avalanches between the electrodes, then the conservation of charge pro-  
 191 duces the system below:

$$192 \quad \begin{cases} n_a &= n_i + n_\gamma \\ n_\gamma &= \gamma(n_b - n_a) \cdot \\ n_b &= A_{\text{av}} n_a \end{cases} \quad (11)$$

193 An electron avalanche occurs when the ratio  $n_b/n_i$  diverges (e.g., Naidu & Kamarju, 2013,  
 194 Sec. 2.5). Then, the condition for initiating a self-sustained discharge follows from Equa-  
 195 tion (8):

$$196 \quad \frac{n_b}{n_i} = \frac{A_{\text{av}}}{1 + \frac{1}{\gamma} - A_{\text{av}}} \rightarrow \infty, \quad (12)$$

199 which is satisfied when:

$$200 \quad A_{\text{av}} = 1 + \frac{1}{\gamma}. \quad (13)$$

202 Using Equation (13) to substitute  $A_{\text{av}}$  in Equation (10) yields after simplifications:<sup>1</sup>

$$203 \quad \boxed{\int_a^b \alpha(E) dr + \ln\left(\frac{\mu(E_a)}{\mu(E_b)}\right) = \ln\left(1 + \frac{1}{\gamma}\right)}. \quad (14)$$

205 In all three 1-D cases, Equations (2), (7a), and (7b) let us approximate  $\alpha/N$  and  
 206  $\mu \times N$  as a function of  $a$ ,  $r$ , and  $E_a$ . Thus, the condition of self-sustainability Equa-

---

<sup>1</sup> Note that if  $E_a = E_b$  (e.g., in a parallel plate geometry), one straightforwardly retrieves the classic for-  
 mula (e.g., Raizer, 1991, p. 177).

207 tion (14) in the absence of space charges and displacement field becomes:

$$208 \int_a^b AN \exp\left(-\frac{B}{E_a/N} \left(\frac{r}{a}\right)^\delta\right) dr + D \ln\left(\left(\frac{b}{a}\right)^\delta\right) = \ln\left(1 + \frac{1}{\gamma}\right) \quad (15)$$

209  
210 If  $A$  and  $B$  are converted to  $1/(\text{cm} \cdot \text{Torr})$  and  $V/(\text{cm} \cdot \text{Torr})$  and  $d$  is the distance be-  
211 tween the electrodes ( $b = a + d$ ), then we can show that the scalability of  $E_a/p$  natu-  
212 rally derives from Equation (15) as follows:

$$213 \int_0^d Ap \exp\left(-\frac{B}{E_a/p} \left(1 + \frac{pr}{pa}\right)^\delta\right) dr + D \ln\left(\left(1 + \frac{pd}{pa}\right)^\delta\right) = \ln\left(1 + \frac{1}{\gamma}\right) \quad (16)$$

215 The critical electric field  $E_{\text{cr}}$  is measured at  $r = a$ , therefore  $E_{\text{cr}} = |E_a|$ . Consequently,  
216 Equation (16) yields the following results for the specific geometries described in Figure 1:

$$218 \exp\left(-\frac{Bp}{E_{\text{cr}}}\right) = \frac{1}{Apd} \ln\left(1 + \frac{1}{\gamma}\right) \quad \delta = 0 \quad (17a)$$

$$219 -\frac{E_{\text{cr}}}{Bp} \left[ \exp\left(-\frac{Bp}{E_{\text{cr}}} \left(1 + \frac{pd}{pa}\right)\right) - \exp\left(-\frac{Bp}{E_{\text{cr}}}\right) \right] = \frac{1}{Apa} \ln\left(\frac{\left(1 + \frac{1}{\gamma}\right)}{\left(1 + \frac{pd}{pa}\right)^D}\right) \quad \delta = 1 \quad (17b)$$

$$220 \sqrt{\frac{E_{\text{cr}}}{Bp}} \left[ \text{erf}\left(\sqrt{\frac{E_{\text{cr}}}{Bp}} \left(1 + \frac{pd}{pa}\right)\right) - \text{erf}\left(\sqrt{\frac{E_{\text{cr}}}{Bp}}\right) \right] = \frac{2}{\sqrt{\pi}} \frac{1}{Apa} \ln\left(\frac{\left(1 + \frac{1}{\gamma}\right)}{\left(1 + \frac{pd}{pa}\right)^{2D}}\right) \quad \delta = 2 \quad (17c)$$

222 where  $\text{erf}(x) = \frac{2}{\sqrt{\pi}} \int_0^x e^{-t^2} dt$  is the Gauss error function (e.g., Lipschutz et al., 2018,  
223 p. 203).

## 224 2.2 Critical voltage

225 Paschen curves are plots of the product pressure times density  $pd$  versus critical  
226 electric potential  $V_{\text{cr}}$ . This potential measured between the electrodes at  $a$  and  $b$  ( $V_{\text{cr}} =$   
227  $V_b - V_a$ ) corresponds to the voltage necessary to initiate a self-sustained discharge and  
228 obeys the classic definition  $V(r) = -\int_a^b \vec{E} \cdot d\vec{r}$  (e.g., Zangwill, 2019, p. 62). Equation (2)  
229 then yields  $V_{\text{cr}}$  for the three cases of Figure 1:

$$230 V_{\text{cr}} = E_{\text{cr}}d \quad \delta = 0 \quad (18a)$$

$$231 V_{\text{cr}} = E_{\text{cr}}a \cdot \ln\left(1 + \frac{d}{a}\right) \quad \delta = 1 \quad (18b)$$

$$232 V_{\text{cr}} = E_{\text{cr}}d \cdot \left(1 + \frac{d}{a}\right)^{-1} \quad \delta = 2 \quad (18c)$$

233

For  $\delta = 0$  (case of parallel plates), Equations (17a) and (18a) simplify into the well-established formula (e.g., Raizer, 1991, p. 133):

$$V_{\text{cr}} = \frac{Bpd}{\ln \left( \frac{Apd}{\ln \left( 1 + \frac{1}{\gamma} \right)} \right)} \quad (19)$$

If Equations (17b) and (17c) had known analytical solutions, one could straightforwardly obtain solutions in the cylindrical and spherical geometries ( $\delta=1$  and  $2$ , respectively) from Equations (18b) and (18c). In the absence of closed-form solutions, we use MATLAB `fzero` root-finding algorithm to numerically solve Equation (17) for  $E_{\text{cr}}$  given specific values of  $pa$  and  $pd$ . This function combines the bisection, secant, and inverse quadratic interpolation methods and is based on the works by Brent (1973) and Forsythe et al. (1976). We use the values of  $E_{\text{cr}}$  to deduce the critical voltage  $V_{\text{cr}}$  from Equation (18) given  $pa$ ,  $pd$ , and  $\delta$ .

In the next section, we present the results from our calculation as surface plots for all three geometries of Figure 1 for the environments described in Table 1. We also compare the results to experimental data from the peer-reviewed literature.

### 3 Results

The near-surface atmospheric breakdown criteria for Earth, Mars, Titan, and Venus are summarized in Figures 3 through 6. In each figure, columns (I) and (II) respectively display the critical electric field  $E_{\text{cr}}$  and potential  $V_{\text{cr}}$  for the various geometries explored here as functions  $pd$  and  $pa$ . The results are displayed for values of  $pa$  from  $10^{-1}$  to  $10^{+3}$  cm · Torr and  $pd$  from  $10^{-1}$  to  $10^{+3}$  cm · Torr. The use of pressure-scaled dimensions eases the comparison with experimental data in columns (III) and (IV). Therefore, Figures 3 to 6 use pressure-scaled values ( $E/p$ ,  $pa$ ,  $pd$ ) rather than number-density scaled parameters (e.g.,  $E/N$ ,  $\alpha/N$ ,  $\mu \times N$  in Figure 2). The conversion is possible using the neutral temperatures given in Table 1 and the ideal gas law discussed in Section 2 (see Appendix A for details).

In Figures 3 to 6, the first, second, and third rows display the results for parallel plates, coaxial cylinders, and concentric spherical electrodes, respectively. Specifically, panels (a) and (b) show the calculated values of  $E_{\text{cr}}$  and  $V_{\text{cr}}$  for the parallel plate geometry and confirm that the critical electric field and potential do not vary as a function

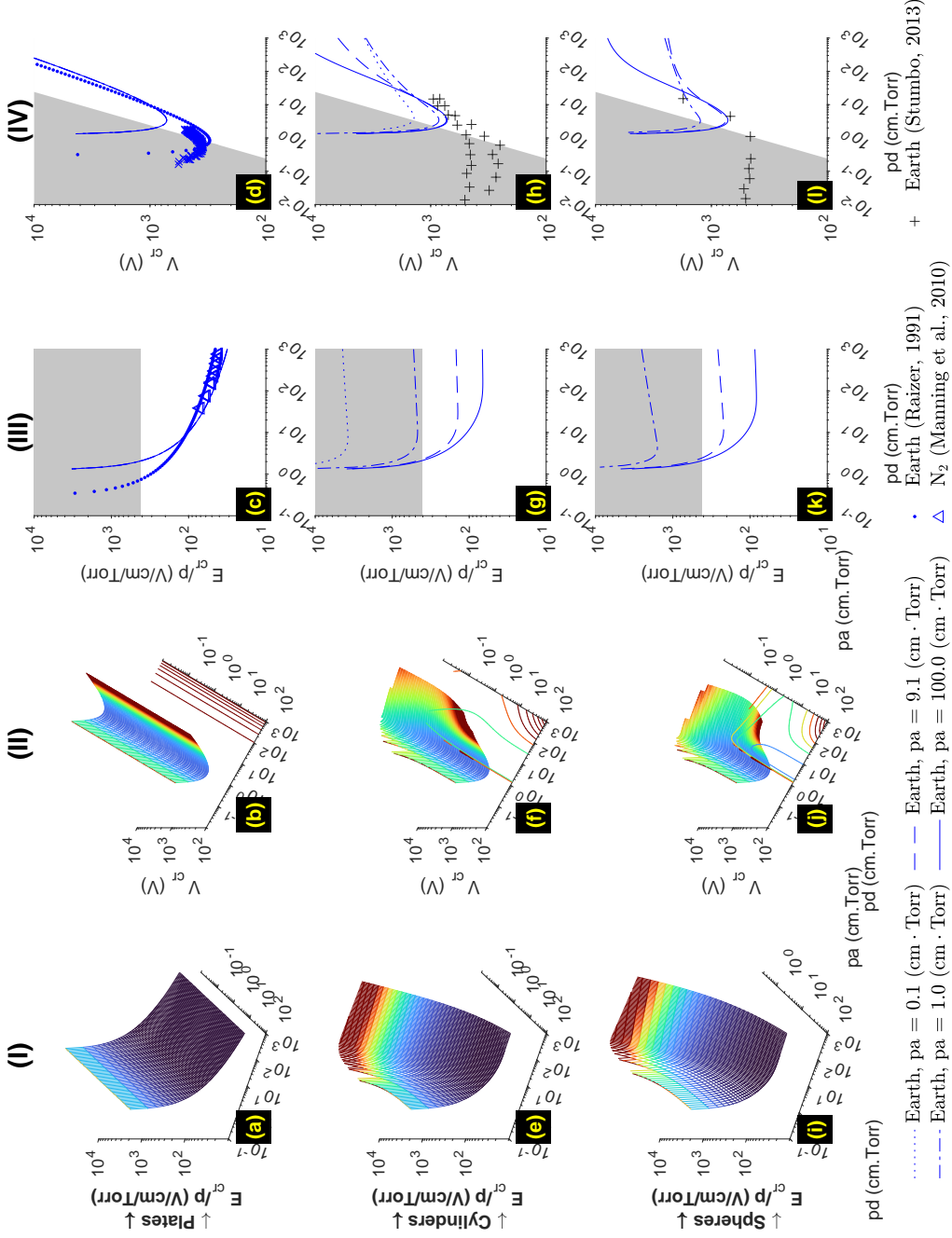


**Figure 3.** Breakdown criteria in the Earth-like atmosphere described in Table 1. The reduced critical electric field  $E_{cr}/p$  is displayed as a function of the reduced size of electrode  $pa$  and distance  $pd$  between electrodes  $a$  and  $b$  in column (I). Column (III) shows  $E_{cr}/p$  vs.  $pd$  for selected  $pa$ -values for comparison with experimental data. Columns (II) and (IV) are the same as columns (I) and (III) but for the critical voltage  $V_{cr}$ . The first, second, and third rows displays the results for electrodes with the following geometries: parallel plates (a-d), coaxial cylinders (e-h), and concentric spheres (i-l). The shaded areas correspond to domains where  $E \geq 10E_k$ .

264 of  $pa$ . Therefore, the surface plots effectively collapse into the well-known curves of Townsend's  
 265 theory. For coaxial cylinders, panels (e) and (f), and concentric spheres, panels (i) and  
 266 (j), Figures 3 to 6 exhibit a similar dependence with  $pd$ , related to the separation between  
 267 the electrodes, but also introduce a new dependence on  $pa$ , emphasizing the role of the  
 268 size of the system for the initiation of self-sustained glow discharge. Conventional Paschen  
 269 curves have a well-defined minimum, Stoletov's point, with a potential  $V_{\min} = \frac{eB}{A} \ln\left(1 + \frac{1}{\gamma}\right)$   
 270 at  $pd_{\min} = \frac{e}{A} \ln\left(1 + \frac{1}{\gamma}\right)$  (e.g., Raizer, 1991, p. 134). However, this minimum point  
 271 becomes a minimum curve in cylindrical and spherical geometries (panels (f) and (j) in  
 272 Figures 3 to 6). As expected, the minimum of the surface plot for the parallel-plate case  
 273 is independent of the value of  $pa$  and obeys Stoletov's equations for  $pd_{\min}$  and  $V_{\min}$ .

274 We compare our numerical results with other numerical calculations and experi-  
 275 mental data in columns (III) and (IV) of Figures 3 to 6. There, we plot selected cross-  
 276 sections from the surface plots in columns (I) and (II). Columns (III) and (IV) display  
 277  $E_{\text{cr}}/p$  and  $V_{\text{cr}}$ , respectively, as a function of the parameter  $pd$  for fixed values of  $pa$ : 0.1,  
 278 1,  $\sim 10$ , and 100 cm·Torr. Experimental measurements in air are rendered in blue mark-  
 279 ers:  $\bullet$  and  $\triangle$  for measurements from (Raizer, 1991) and  $\times$  for Stumbo's (2013) data. Red  
 280 markers display data for Mars:  $\nabla$  for Raizer's (1991) and  $+$  for Manning, ten Kate, Bat-  
 281 tel, and Mahaffy's (2010) works. We further show data for pure CO<sub>2</sub> with black mark-  
 282 ers where  $\bullet$ ,  $\square$ ,  $\nabla$ ,  $+$ ,  $\times$ , and  $\triangleleft$  show the results from (Raizer, 1991), (Hackam, 1969),  
 283 (Buhler et al., 2003), (Manning et al., 2010), (Stumbo, 2013), and (Meek & Craggs, 1953),  
 284 respectively. For comparisons with Earth and Titan scenarios, we included experimen-  
 285 tal results in N<sub>2</sub> from (Manning et al., 2010).

286 As expected, self-sustained discharges between parallel plates do not depend on the  
 287 parameter  $pa$  (see panels (a) and (b) across Figures 3 through 6). Interestingly, Stole-  
 288 tov's points visible in column (IV) occur at similar values of  $pd$  and  $V_{\min}$  ( $\approx 0.1 - 1$  cm · Torr  
 289 and  $\approx 2$  V/cm/Torr, respectively) for the various gas mixtures and geometries. Columns  
 290 (III) and (IV) also show that the theoretical values from Section 2 underestimate exper-  
 291 imental values of  $E_{\text{cr}}$  and  $V_{\text{cr}}$  for all geometries and values of  $pa$ . For a given system, if  
 292 one splits the Paschen curve around the Stoletov's point, one can define a high electric  
 293 field regime for  $pd \ll pd_{\min} \approx 0.1 - 1$  cm · Torr forming the left-hand branch of the  
 294 curves and a high-pressure regime on the right-hand branch of curves for  $pd \gtrsim pd_{\min}$ .

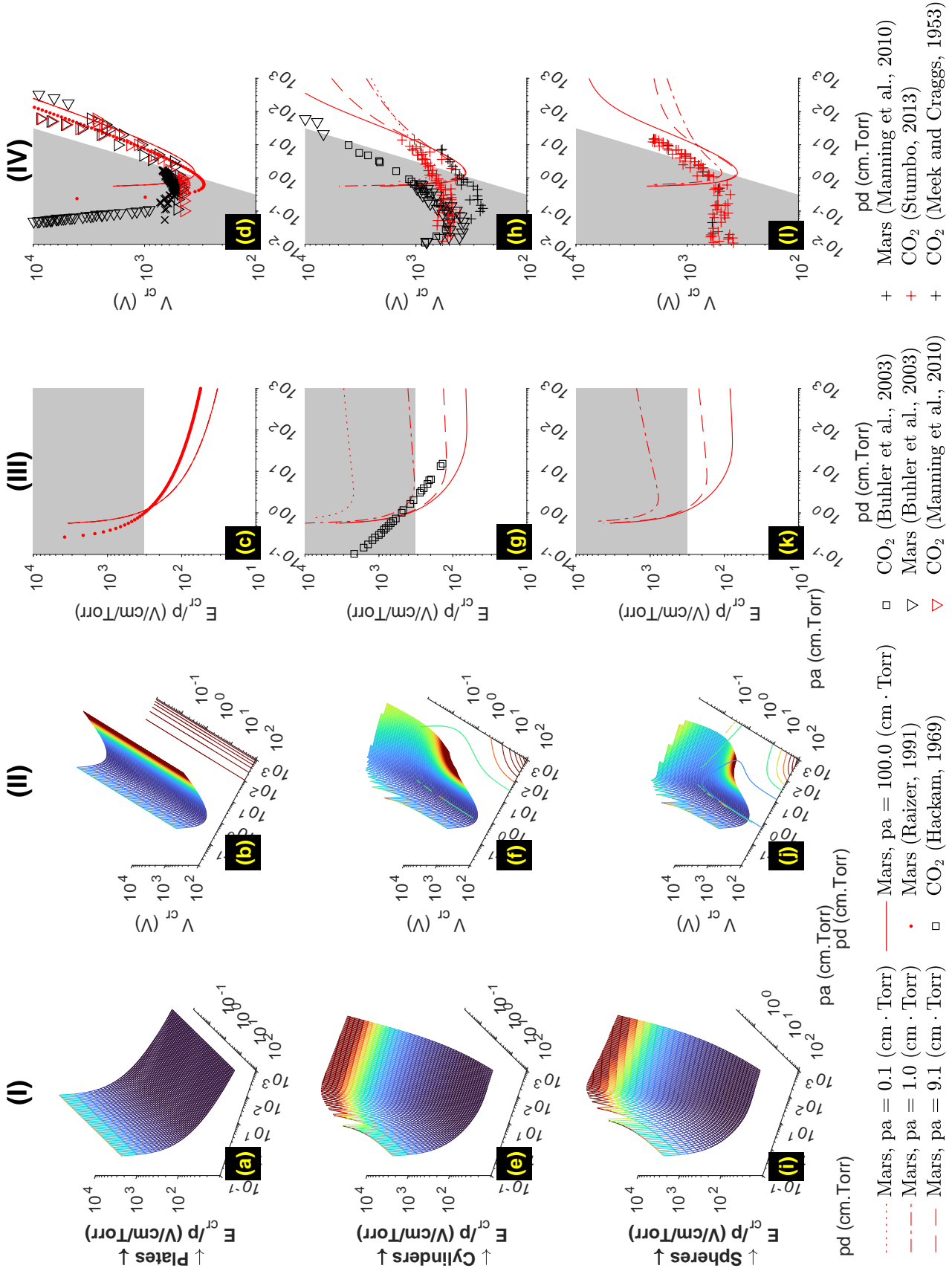


Figure 4. Same as Figure 3 for the Mars-like environment described in Table 1.

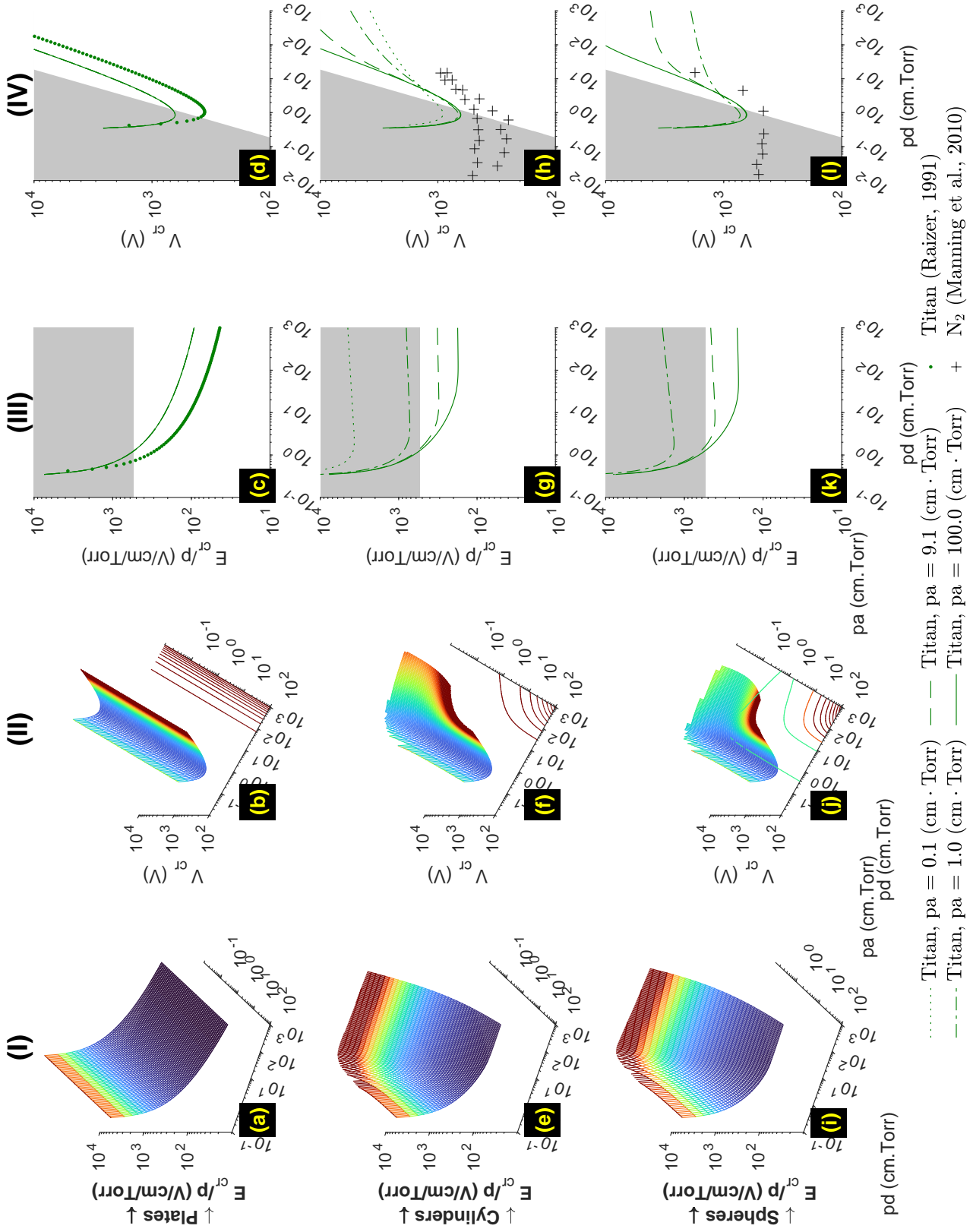


Figure 5. Same as Figure 3 for the Titan-like environment described in Table 1.

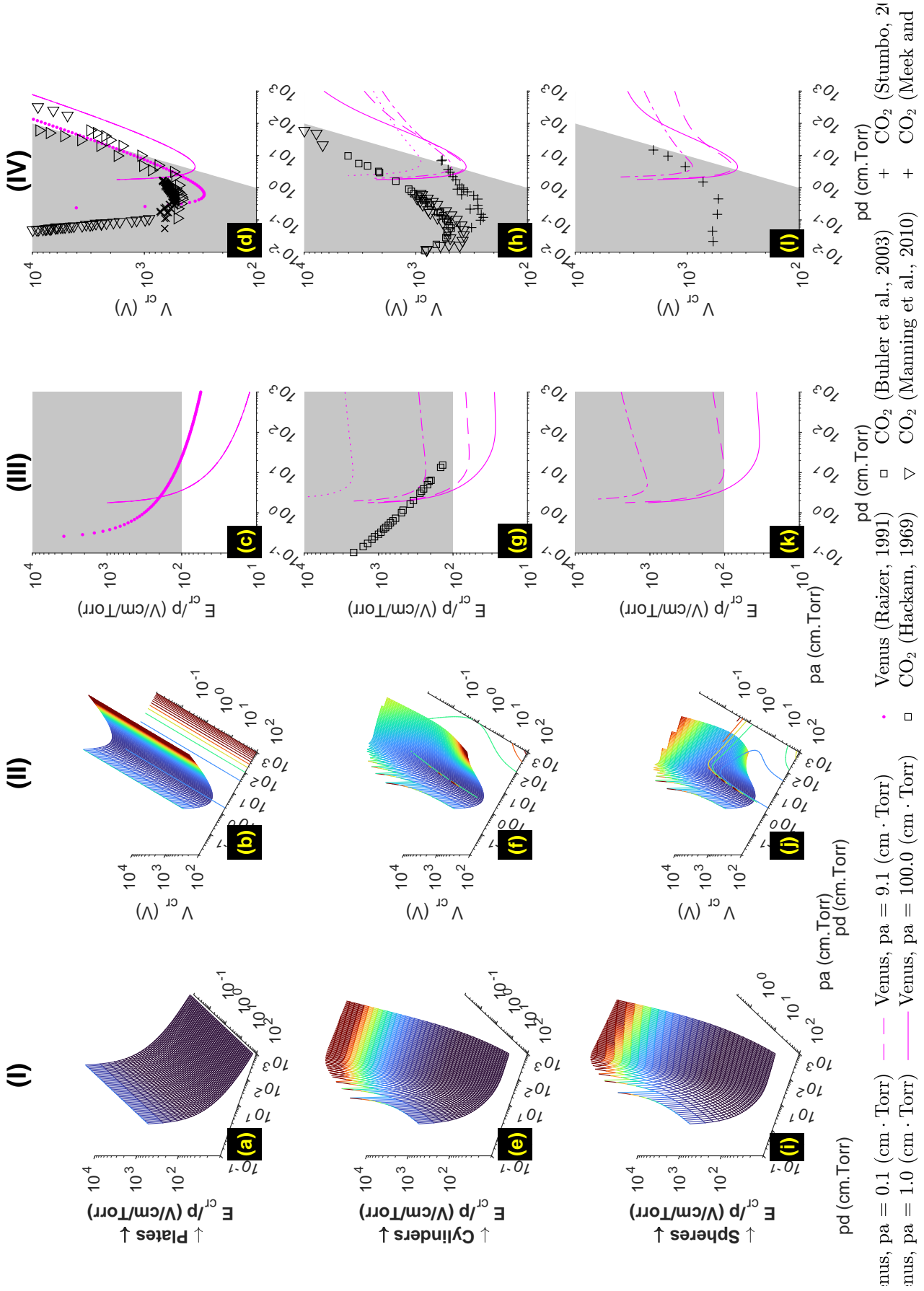


Figure 6. Same as Figure 3 for the Venus-like environment described in Table 1.

295 The right branches of the curves show promising agreement (within an order of mag-  
 296 nitude) between theoretical curves and measurements provided that: (1) one accounts  
 297 for the uncertainty in deriving the coefficients  $A$ ,  $B$ , and  $D$ ; and (2) one carefully con-  
 298 sider the values of  $pa$  best representing the geometries of concentric or coaxial electrodes.  
 299 For these reasons, we shall note that the theoretical slopes closely follow those formed  
 300 by the experimental measurements from various authors (see legends of Figures 3 through  
 301 6 for details). The curves using  $A$  and  $B$  from (Raizer, 1991, p. 56 and ‘•’ markers in  
 302 columns (III) and (IV)) show the influence of these coefficients on the location of Sto-  
 303 letov’s points in theoretical plots. While some authors have derived these values directly  
 304 from the Paschen curves, we derived  $A$ ,  $B$ , and  $D$  from solutions to the Boltzmann equa-  
 305 tion (see Figure 2 and Section 2) to maintain consistency of methodology across coeffi-  
 306 cients and gases. Another explanation of the aforementioned difference stems from the  
 307 differences between pure gases and complex atmospheres (e.g., pure  $\text{CO}_2$  vs. Mars at-  
 308 mospheres, pure  $\text{N}_2$  vs air). Even in cases when the atmospheric composition is almost  
 309 pristine (e.g., Mars’s atmosphere is  $\gtrsim 95\%$   $\text{CO}_2$ ), the presence of minor components  
 310 can dramatically alter the condition for discharge initiation as evidenced by Rioussset et  
 311 al. (2020) in the case of conventional breakdown  $E_k$ .

## 312 4 Discussion

313 The results presented in Section 3 differ from previous attempts at generalizing Townsend’s  
 314 theory of Paschen curves mainly in their full treatment of electron mobility in the con-  
 315 tinuity equation. Neglecting the volume increase along the avalanche path, Raizer (1991,  
 316 p. 177) or Meek and Craggs (1953, p. 100) straightforwardly rewrote the condition for  
 317 initiation of self-sustained discharges Equation (15) as:  $\int_a^b Ap \exp(-Bp/E(r)) dr = \ln(1 + 1/\gamma)$ .  
 318 The proposed formalism here includes the volume change as the electrons move from the  
 319 inner to the outer electrode via the additional mobility term:  $\ln(\mu(E_a)/\mu(E_b)) \approx D \ln((b/a)^\delta)$ .

320 Section 2 has established the equivalence between the classic theory for parallel plate  
 321 electrodes and the equations developed in this work. In addition, the revised equations  
 322 are fully consistent with the well-established scaling laws. We further note that all the  
 323 geometrical parameters in Equation (16) appear in a product with  $p$  (i.e.,  $pa$ ,  $pb$ ,  $pr$ , and  
 324  $pd$ ). Consequently, one must have  $E_{cr} \propto p$  so that Equation (16) remains true if the  
 325 pressure changes with all other parameters remaining the same. Similarly, Equation (18)  
 326 establishes the invariance of the critical voltage  $V_{cr}$  through pressure changes. Writing

327  $E_{\text{cr}} = \frac{E_{\text{cr}}}{p}p$  lets us rewrite Equations (18a), (18b), and (18c) to display the pressure  
 328 scaling explicitly as follows:

$$329 \quad V_{\text{cr}} = \frac{E_{\text{cr}}}{p}pa \cdot \frac{pd}{pa} \quad \delta = 0 \quad (20a)$$

$$330 \quad V_{\text{cr}} = \frac{E_{\text{cr}}}{p}pa \cdot \ln \left( 1 + \frac{pd}{pa} \right) \quad \delta = 1 \quad (20b)$$

$$331 \quad V_{\text{cr}} = \frac{E_{\text{cr}}}{p}pa \cdot \frac{\frac{pd}{pa}}{1 + \frac{pd}{pa}} \quad \delta = 2 \quad (20c)$$

332  
 333 Since  $E_{\text{cr}}/p$  is constant, then  $V_{\text{cr}}$  only depends on the parameters  $pd$  (as in the classic  
 334 Townsend's (1901) theory) and  $pa$ . The previously established scaling law stands with  
 335 the additional parameter  $pa$ . Therefore, Equations (17) and (20) demonstrate that both  
 336 the critical electric field,  $E_{\text{cr}}$ , and potential,  $V_{\text{cr}}$ , are functions of the reduced electrode  
 337 and gap sizes, namely  $pa$  and  $pd$ .

338 Alternately, the ideal gas law,  $p = Nk_{\text{B}}T$ , allows us to rewrite  $E_{\text{cr}}$  and  $V_{\text{cr}}$  as func-  
 339 tions of  $Nd$  and  $Na$ , where  $N$  is the number gas density. This result holds for constant  
 340 gas temperature, which is a reasonable assumption for a cold, non-thermalized discharge  
 341 such as corona or glow. However, it is worth noting that the coefficients  $A$ ,  $B$ , and  $D$   
 342 are derived from a fit to the Boltzmann equation using the parameters given in Table 1.  
 343 The BOLSIG+ solver (Hagelaar, 2015) requires a temperature input while it outputs re-  
 344 duced values for  $\alpha$  and  $\mu$  using the number density  $N$ . The pressure conversion is nec-  
 345 essary to compare to experimental data. The temperatures we used for the four worlds  
 346 are summarized in Table 1. The conversions of the coefficients from density to pressure  
 347 call for the neutral gas temperature (see Appendix A) and this information is required  
 348 for direct comparison between experimental and theoretical Paschen curves. Any mod-  
 349 ification to the  $A$  and  $B$  coefficients will primarily shift the curves and surfaces along  
 350 the vertical  $V_{\text{cr}}$  and horizontal  $pd$  axes of Figures 3 to 6, respectively.

351 In all considered cases,  $E_{\text{cr}}/p$  and  $V_{\text{cr}}$  present an asymptotic behavior towards in-  
 352 finite electric field and potential for low values of  $pd$ , independently of  $pa$ . The values  
 353 on the left branches of the Paschen curves ( $pd \lesssim pd_{\text{min}}$  in column (IV) of Figures 3  
 354 through 6) should be taken with caution as they may not describe the physical mech-  
 355 anism occurring in high-electric fields. Discharges at very low  $pd$  correspond to dielec-  
 356 tric breakdown in a quasi-vacuum. Indeed, Raizer (1991, p. 135) noticed that the electron-  
 357 avalanche process responsible for self-sustained discharges between parallel plates is re-

358 placed by cathode emission at  $pd \lesssim 10^{-3} \text{ cm} \cdot \text{Torr}$ . Thus, the properties of the dis-  
 359 charge are no longer defined by the neutral gas between the electrode, but rather by the  
 360 metallic composition of the electrode. For this reason, the numerical solutions presented  
 361 in this work do not apply in such regimes. On the other hand, the convergence across  
 362 gas compositions at high  $pd$  indicates that the number density of the neutral gas can be-  
 363 come a dominant factor over the molecular electric properties for large gaps under sig-  
 364 nificant pressure. The right branches show similarities to each other across the geome-  
 365 tries at large  $pd \lesssim 100 \text{ cm} \cdot \text{Torr}$ . We advance that these similarities (observed in col-  
 366 umn (IV) of Figures 3 through 6) reflect a regime where the electrode radii of curvature  
 367 are large enough relative to the gap sizes to result in quasi-plane-to-plane conditions.

368 Considering the uncertainty of the electrode geometries in experimental data, the  
 369 theoretical curves are consistent with the measurements. Both approaches indicate min-  
 370 ima in the critical voltages around  $0.5 \text{ cm} \cdot \text{Torr}$ . A simple division by the atmospheric  
 371 pressure returns the gap size most susceptible to trigger a self-sustained discharge in a  
 372 given atmosphere. For example, under a pressure of 760 Torr (Earth’s surface pressure),  
 373 dielectric breakdown may occur in gaps sizes  $\approx 5 \mu\text{m}$  at  $V_{\text{cr}} \lesssim 500 \text{ V}$ . At tropopause’s  
 374 levels,  $p \approx 200 \text{ Torr}$  and the same voltage can initiate a Townsend discharge in a larger  
 375 gap ( $d \approx 25 \mu\text{m}$ ). Similarly, the lower pressure in the Martian atmosphere indicates  
 376 that larger gaps are more prone to dielectric breakdown at the surface of Mars.

377 Panels (f) and (j), i.e., Column (II), of Figures 3 to 6 emphasize the added role of  
 378 mobility in non-planar geometries. In particular, these plots suggest that a reduced ra-  
 379 dius  $pa$  of  $\approx 1 \text{ cm} \cdot \text{Torr}$  is better for initiating self-sustained glow discharges. This cor-  
 380 responds to radii of curvatures  $a \approx 0.05/1 \text{ mm}$  for Earth and  $0.2/5 \text{ mm}$  for Mars at  
 381 ground and cloud levels ( $z \approx 10/20 \text{ km}$ ) in the atmosphere. Such radii of curvature  
 382 are consistent with previous theories that sharp-tipped rods should facilitate the initi-  
 383 ation of upward-connecting leaders and result in better lightning protection, a predic-  
 384 tion contrary to field studies (e.g., Moore, 1983; Moore, Aulich, & Rison, 2000; Moore,  
 385 Rison, et al., 2000; Moore et al., 2003). The paradox therefore remains. However, for Earth,  
 386 the previous calculations indicate that millimeter-sized ice graupels are in the ideal size  
 387 range for discharge initiation at cloud altitude. Beyond meteorological multiphase flows,  
 388 numerous Earth systems transport particles in these size ranges and involve discharges  
 389 processes across a wide range of scales (Crozier, 1964; Kamra, 1972; W. M. Farrell et al.,  
 390 2004; Cimarelli et al., 2022; Méndez Harper et al., 2022). Such flows include gravity cur-

391 rents (dust storms, pyroclastic density currents), volcanic eruption plumes, and wildfire  
392 smoke clouds. Particles in these contexts may have substantial inertia and granular tem-  
393 peratures such that transient optimal gap distances between particles should be common  
394 even in very dilute flows (Dufek et al., 2012; Dufek & Bergantz, 2007). Lastly, if corona  
395 discharge is indeed a precursor to connecting leaders, they can be involved in the pro-  
396 cess of initiation of lightning and Transient Luminous Events (TLEs), jets and sprites  
397 in particular.

398 While this study provides a framework to constrain the capacity of charged surfaces  
399 to cause a breakdown on Mars, Titan, and Venus, how surfaces become electrified on these  
400 worlds remains an area of active research. Mars, for instance, lacks a hydrological cycle  
401 to drive meteorological electrical activity analogous to that on Earth. While Titan and  
402 Venus do have “hydrological” processes that involve the cycle of hydrocarbons and sul-  
403 fur compounds, respectively, whether or not clouds of these compositions are propitious  
404 for discharges remains unknown (Hayes et al., 2018; Shao et al., 2020).

405 However, as is the case for Earth, the three other worlds considered here do host  
406 granular reservoirs that could provide pathways for non-meteorological discharges (Thomas  
407 & Gierasch, 1985; Balme & Greeley, 2006; Radebaugh et al., 2008; Lorenz & Zimbelman,  
408 2014). Martian dust storms involve the movement of large amounts of silicate particles  
409 which invariably undergo collisions. These interactions could charge dust particles via  
410 frictional and contact electrification—collectively known as *triboelectrification* (Horányi  
411 & Lawrence, 2001; Melnik & Parrot, 1998; Merrison et al., 2004; Delory & Farrell, 2011).  
412 Indeed, a broad range of experimental efforts suggests that tribocharging may be quite  
413 efficient within Martian dust events (e.g., Eden & Vonnegut, 1973; Krauss et al., 2003;  
414 Wurm et al., 2019; Méndez Harper et al., 2021). While these experiments have investi-  
415 gated electrification at the grain scale, computer simulations (sometimes combined with  
416 experiments (e.g., Harrison et al., 2016)) have provided useful full-scale expedients for  
417 studies of dust devil electrification (e.g., Melnik & Parrot, 1998; W. M. Farrell et al., 2003).  
418 The results of these studies all converge to the conclusion that electrification in Martian  
419 dust storms should suffice to produce gas breakdown and an atmospheric electric circuit  
420 (W. M. Farrell & Desch, 2001).

421 Similar charging processes may operate on Titan and Venus (or any other world  
422 with mobile granular materials). On Titan, triboelectrification has been associated with

423 the transport of wind-blown hydrocarbon sand (Méndez Harper et al., 2017) and the ag-  
 424 gregation of fine photochemical hazes. Very little work has explored triboelectrification  
 425 under relevant Venusian conditions. However, the presence of dunes and volcanic features  
 426 on Venus indicates particles may charge frictionally during aeolian transport and erup-  
 427 tions (James et al., 2008).

428 Determining the conditions under which atmospheric discharges occur has impli-  
 429 cations for atmospheric chemistry and habitability. Furthermore, discharges could present  
 430 risks to landers and rovers or cause artifacts that confound the interpretation of sensor  
 431 data (Krauss et al., 2003). Recently, for instance, calculations performed by W. Farrell  
 432 et al. (2021) suggest that the rotors of the Ingenuity helicopter could cause localized break-  
 433 down during landing or takeoff. While videography of initial flights has not revealed vi-  
 434 sual evidence for discharges, such events may be best detected electronically. Unfortu-  
 435 nately, Ingenuity does not have the instrumentation to make such measurements. The  
 436 upcoming Dragonfly rotorcraft mission to Titan, however, will involve an electric field  
 437 measurement system (EFIELD) in its DraGMet suite. The main objective of the EFIELD  
 438 experiments is to measure Schumann resonances, which, if detected, would provide ev-  
 439 idence for lightning. Beyond ELF modes, Chatain et al. (2022) have made a compelling  
 440 case that the sensor could be used to detect the movement of charged hydrocarbon sand  
 441 flying past or impinging on the probe during “brownout” conditions. Because (by def-  
 442 inition) discharges also involve the movement of charge, the EFIELD instrument could,  
 443 in principle, detect small-scale breakdown in the vicinity of the rotorcraft. In the case of  
 444 Venus, near-term investigations of discharges in the Venusian environment will remain  
 445 limited to remote sensing observations and analog experiments.

## 446 5 Conclusions

447 The principal results and contributions from this work can be summarized as fol-  
 448 lows:

- 449 1. The theoretical treatment of self-sustained discharge between coaxial cylinders or  
 450 concentric spheres requires a model of mobility. The reduced electron mobility in  
 451 telluric world atmospheres approximately follows a power law:  $\tilde{\mu} \times N = C(E/N)^D$ ,  
 452 where  $C$  and  $D$  are gas-specific constants derived from a numerical fit to the curve  
 453  $E/N$  vs.  $\mu \times N$ .

- 454 2. The newly proposed formalism explains the slope of the Paschen curves in non-  
 455 planar geometries and maintains the scaling laws established by the classic the-  
 456 ory.
- 457 3. In cylindrical and spherical cases, both electrode and gap sizes define the condi-  
 458 tion of discharge initiation. Thus, Paschen curves and Stoletov's points become  
 459 surfaces and curves, respectively.
- 460 4. Critical voltages occur at  $pd$  and  $pa \approx 0.5 \text{ cm} \cdot \text{Torr}$ , suggesting easier initiation around  
 461 millimeter-size particles in dust and water clouds.
- 462 5. Glow corona formation is easier in Mars low pressure,  $\text{CO}_2$ -rich atmosphere than  
 463 in Earth's high-pressure atmosphere.

464 The specific values of the fit coefficients need revising based on laboratory exper-  
 465 iments rather than numerical experiments (i.e., solution of the Boltzmann equation) and  
 466 will be addressed in future work.

## 467 Appendix A Density vs. pressure scaling

468 Experimental work typically adopts pressure-scaled variable,  $E/p$ ,  $\alpha/p$ ,  $\mu \times p$  (e.g.,  
 469 columns (III) and (IV) in Figures 3 to 6), while numerical solvers conventionally prefer  
 470 the number density  $N$  as the scaling factor. Calculations of the fit coefficients  $A$ ,  $B$ ,  $C$ ,  
 471 and  $D$  are performed using numerical solutions but require conversion for comparison  
 472 with the peer-reviewed experimental data. Equations (A1) to (A3) provide the conver-  
 473 sion factors.

$$474 \quad \frac{\alpha}{p} = \left( \frac{101325}{100 \cdot 760} \cdot \frac{1}{k_B T} \right) \frac{\alpha}{N} \quad (\text{A1})$$

$$475 \quad \mu \times p = \left( \frac{10^4 \times 760}{101325} \cdot k_B T \right) \mu \times N \quad (\text{A2})$$

$$476 \quad \frac{E}{p} = \left( \frac{101325 \cdot 10^{-21}}{100 \cdot 760} \cdot \frac{1}{k_B T} \right) \frac{E}{N} \quad (\text{A3})$$

478 where the variables have the units indicated in parentheses:  $\alpha/p$  ( $1/(\text{cm} \cdot \text{Torr})$ ),  $\mu \times$   
 479  $p$  ( $(\text{cm}^2 \cdot \text{Torr}) / (\text{V} \cdot \text{s})$ ),  $E/p$  ( $\text{V}/(\text{cm} \cdot \text{Torr})$ ),  $\alpha/N$  ( $\text{m}^2$ ),  $\mu \times N$  ( $1/(\text{V} \cdot \text{m} \cdot \text{s})$ ),  $E/N$  ( $\text{Td}$ ),  
 480  $k_B$  ( $\text{J}/\text{K}$ ), and  $T$  ( $\text{K}$ ), respectively.

481 Similarly, the fit coefficients  $A$  and  $B$  need converting. If indices  $p$  and  $N$  indicate  
 482 the variables used for density and pressure calculations, then:

$$483 \quad A_p = \left( \frac{101325}{100 \cdot 760} \cdot \frac{1}{k_B T} \right) A_N \quad (\text{A4})$$

$$484 \quad B_p = \left( \frac{101325 \cdot 10^{-21}}{100 \cdot 760} \cdot \frac{1}{k_B T} \right) B_N \quad (\text{A5})$$

486 The coefficient  $D$  is unchanged, while  $C$  cancels out from the equations and requires no  
 487 conversion.

## 488 Acknowledgment

489 This work was supported by the National Science Foundation (grant number: 2047863).  
 490 The authors also acknowledge Embry-Riddle Aeronautical University Office of Under-  
 491 graduate Research for supporting Mr. Jacob A. Engle initial contribution to this work.

## 492 Open Research Statement

493 Software for this research is available in these in-text data citation references: (Riousset,  
 494 2022, v1.0.2) under GNU General Public License Version 3, 29 June 2007. Boltzmann's  
 495 equation solver, namely BOLSIG+ is fully described in (Pancheshnyi et al., 2012; Pitch-  
 496 ford et al., 2016; Carbone et al., 2021).

497 The cross-section data used for solving Boltzmann's equation in the study are ob-  
 498 tained from:

- 499 • Hayashi database, [www.lxcat.net](http://www.lxcat.net), retrieved on May 24, 2019.
- 500 • Morgan database, [www.lxcat.net](http://www.lxcat.net), retrieved on May 24, 2019.

501 and available from (Riousset, 2022, v1.0.2).

## 502 CRediT

503 **Jérémy A Riousset:** Conceptualization, Methodology, Software, Formal Anal-  
 504 ysis, Investigation, Resources, Data Curation, Writing - Original draft preparation, Vi-  
 505 sualization, Supervision, Project Administration, Funding Acquisition **Joshua S. Méndes-**  
 506 **Harper:** Validation, Formal Analysis, Investigation, Writing - Original draft prepara-  
 507 tion, Visualization, Funding Acquisition **Josef Dufek:** Validation, Formal Analysis, In-  
 508 vestigation, Resources, Writing - Original draft preparation, Supervision, Project Admin-

509 istration, Funding Acquisition **Jared P. Nelson**: Validation, Formal Analysis, Inves-  
 510 tigation, Writing - Review & Editing **Annelisa B. Esparza**: Investigation, Data Cu-  
 511 ration, Writing - Review & Editing.

## 512 **References**

- 513 Balme, M., & Greeley, R. (2006). Dust devils on Earth and Mars. *Rev. Geophys.*,  
 514 *44*(3). doi: 10.1029/2005rg000188
- 515 Bazelyan, E. M., & Raizer, Y. P. (1998). *Spark Discharge*. New York, NY: Chemical  
 516 Rubber Company Press.
- 517 Bering, E. A., Benbrook, J. R., Bhusal, L., Garrett, J. A., Paredes, A. M., Wescott,  
 518 E. M., . . . Lyons, W. A. (2004). Observations of transient luminous events  
 519 (TLEs) associated with negative cloud to ground (-CG) lightning strokes.  
 520 *Geophys. Res. Lett.*, *31*(5). (L05104) doi: 10.1029/2003GL018659
- 521 Brent, R. P. (1973). *Algorithms for Minimisation without Derivatives*. Englewood  
 522 Cliffs, NJ: Prentice-Hall.
- 523 Buhler, C. R., Calle, C. I., & Nelson, E. (2003, March). Electrical breakdown in a  
 524 Martian gas mixture. In S. Mackwell & E. Stansbery (Eds.), *LPSC* (Vol. 34).  
 525 League City, TX.
- 526 Carbone, E., Graef, W., Hagelaar, G., Boer, D., Hopkins, M. M., Stephens, J. C.,  
 527 . . . Pitchford, L. (2021, February). Data needs for modeling low-temperature  
 528 non-equilibrium plasmas: The LXCat project, history, perspectives and a  
 529 tutorial. *Atoms*, *9*(1), 16. doi: 10.3390/atoms9010016
- 530 Chatain, A., Le Gall, A., Berthelier, J.-J., Lorenz, R. D., Hassen-Khodja, R., Lebre-  
 531 ton, J.-P., . . . Déprez, G. (2022). Detection and characterization of wind-blown  
 532 charged sand grains on titan with the dragmet/efield experiment on dragonfly.  
 533 *Icarus*, 115345.
- 534 Chen, F. F. (1984). *Introduction to Plasma Physics and Controlled Fusion*. New York:  
 535 Plenum Press.
- 536 Cimarelli, C., Behnke, S., Genareau, K., Harper, J. M., & Van Eaton, A. R. (2022).  
 537 Volcanic electrification: recent advances and future perspectives. *Bulletin of Vol-*  
 538 *canology*, *84*(8), 1–10.
- 539 Crozier, W. D. (1964, December). The electric field of a New Mexico dust devil. *J.*  
 540 *Geophys. Res.*, *69*(24), 5427–5429. doi: 10.1029/JZ069i024p05427

- 541 Delory, G., & Farrell, W. (2011). Atmospheric electricity on Mars. In *Epsc-dps joint*  
542 *meeting* (Vol. 6, p. 1229).
- 543 Déprez, G., Montmessin, F., Witasse, O., Lapauw, L., Vivat, F., Abbaki, S., ...  
544 Barth, E. (2014, May). Micro-ARES, an electric-field sensor for ExoMars 2016:  
545 Electric fields modelling, sensitivity evaluations and end-to-end tests. In *Egu*  
546 *general assembly conference abstracts* (Vol. 16, p. 16613).
- 547 Dubrovin, D., Nijdam, S., van Veldhuizen, E. M., Ebert, U., Yair, Y., & Price, C.  
548 (2010, June). Sprite discharges on Venus and Jupiter-like planets: A laboratory  
549 investigation. *J. Geophys. Res.*, *115*(A6). doi: 10.1029/2009ja014851
- 550 Dufek, J., & Bergantz, G. (2007). Suspended load and bed-load transport of particle-  
551 laden gravity currents: the role of particle–bed interaction. *Theoretical and*  
552 *Computational Fluid Dynamics*, *21*(2), 119–145.
- 553 Dufek, J., Manga, M., & Patel, A. (2012). Granular disruption during explosive vol-  
554 canic eruptions. *Nature Geoscience*, *5*(8), 561–564.
- 555 Eden, H. F., & Vonnegut, B. (1973). Electrical breakdown caused by dust motion in  
556 low pressure atmospheres: Considerations for Mars. *Nature*, *280*, 962.
- 557 Farrell, W., McLain, J., Marshall, J., & Wang, A. (2021). Will the mars helicopter  
558 induce local martian atmospheric breakdown? *The Planetary Science Journal*,  
559 *2*(2), 46.
- 560 Farrell, W. M., Delory, G. T., Cummer, S. A., & Marshall, J. R. (2003, October). A  
561 simple electrodynamic model of a dust devil. *Geophys. Res. Lett.*, *30*(20), 2050.  
562 doi: 10.1029/2003GL017606
- 563 Farrell, W. M., & Desch, M. D. (2001, April). Is there a Martian atmospheric electric  
564 circuit? *J. Geophys. Res.*, *106*, 7591–7596. doi: 10.1029/2000JE001271
- 565 Farrell, W. M., Smith, P. H., Delory, G. T., Hillard, G. B., Marshall, J. R., Catling,  
566 D., ... Johnson, B. (2004). Electric and magnetic signatures of dust devils from  
567 the 2000–2001 MATADOR desert tests. *J. Geophys. Res.*, *109*(E3). (E03004)  
568 doi: 10.1029/2003JE002088
- 569 Forsythe, G. E., Malcolm, M. A., & Moler, C. B. (1976). *Computer Methods for Math-*  
570 *ematical Computations*. Englewood Cliffs, NJ: Prentice-Hall.
- 571 Hackam, R. (1969, February). Total secondary ionization coefficients and breakdown  
572 potentials of hydrogen, methane, ethylene, carbon monoxide, nitrogen, oxygen  
573 and carbon dioxide between mild steel coaxial cylinders. *J. Phys. B: At. Mol.*

- 574 *Phys.*, 2(2), 216–233. doi: 10.1088/0022-3700/2/2/309
- 575 Hagelaar, G. J. M. (2015, December). Coulomb collisions in the Boltzmann equa-  
576 tion for electrons in low-temperature gas discharge plasmas. *Plasma Sources Sci.*  
577 *Technol.*, 25(1), 015015. doi: 10.1088/0963-0252/25/1/015015
- 578 Harrison, R. G., Barth, E., Esposito, F., Merrison, J., Montmessin, F., Aplin, K. L.,  
579 ... Zimmerman, M. (2016, April). Applications of electrified dust and dust  
580 devil electrodynamics to Martian atmospheric electricity. *Space Sci. Rev.*,  
581 203(1-4), 299–345. doi: 10.1007/s11214-016-0241-8
- 582 Hayes, A. G., Lorenz, R. D., & Lunine, J. I. (2018). A post-cassini view of titan’s  
583 methane-based hydrologic cycle. *Nature Geoscience*, 11(5), 306–313.
- 584 Hess, B. L., Piazzolo, S., & Harvey, J. (2021). Lightning strikes as a major facilita-  
585 tor of prebiotic phosphorus reduction on early earth. *Nature communications*,  
586 12(1), 1–8.
- 587 Horányi, M., & Lawrence, G. (2001). Charged dust currents on the surface of Mars.  
588 *Phys. Scr.*, 89, 130–132. doi: 10.1238/Physica.Topical.089a00130
- 589 Hörst, S. M. (2017). Titan’s atmosphere and climate. *Journal of Geophysical Re-*  
590 *search: Planets*, 122(3), 432–482.
- 591 Jakosky, B. M., Grebowsky, J. M., Luhmann, J. G., Connerney, J., Eparvier, F., Er-  
592 gun, R., ... Yelle, R. (2015, November). MAVEN observations of the response  
593 of Mars to an interplanetary coronal mass ejection. *Science*, 350, 0210. doi:  
594 10.1126/science.aad0210
- 595 Jakosky, B. M., Lin, R. P., Grebowsky, J. M., Luhmann, J. G., Mitchell, D., Beu-  
596 telschies, G., ... others (2015). The mars atmosphere and volatile evolution  
597 (maven) mission. *Space Science Reviews*, 195(1), 3–48.
- 598 James, M., Wilson, L., Lane, S., Gilbert, J., Mather, T., Harrison, R., & Martin, R.  
599 (2008). Electrical charging of volcanic plumes. *Space Science Reviews*, 137(1),  
600 399–418.
- 601 Justh, H., & Hoffman, J. (2020). Titan global reference atmospheric model (titan-  
602 gram): User guide.
- 603 Justh, H. L., & Dwyer Cianciolo, A. (2021, January). Venus Global Reference At-  
604 mospheric Model (Venus-GRAM) updates. In *43rd COSPAR scientific assem-*  
605 *bly* (Vol. 43, p. 429). Retrieved from [https://ui.adsabs.harvard.edu/abs/](https://ui.adsabs.harvard.edu/abs/2021cosp...43E.429J)  
606 2021cosp...43E.429J (28 January - 4 February)

- 607 Justh, H. L., Justus, C. G., & Badger, A. M. (2010). Updating Mars-GRAM to in-  
 608 crease the accuracy of sensitivity studies at large optical depths. In *COSPAR*  
 609 *Scientific Assembly* (Vol. 38, p. 4).
- 610 Kamra, A. (1972). Physical sciences: Visual observation of electric sparks on gypsum  
 611 dunes. *Nature*, *240*(5377), 143–144.
- 612 Krauss, C. E., Horányi, M., & Robertson, S. (2003, June). Experimental evidence for  
 613 electrostatic discharging of dust near the surface of Mars. *New J. Phys.*, *5*, 70.  
 614 doi: 10.1088/1367-2630/5/1/370
- 615 Leblanc, F., Aplin, K., Yair, Y., Harrison, G., Lebreton, J. P., & Blanc, M. (Eds.).  
 616 (2008). *Planetary Atmospheric Electricity*. New York, NY: Springer-Verlag  
 617 GmbH.
- 618 Leslie, F. (2008). Earth Global Reference Atmospheric Model 2007 (Earth-GRAM07).  
 619 In *COSPAR Scientific Assembly* (Vol. 37, p. 1748).
- 620 Lieberman, M. A., & Lichtenberg, A. J. (2005). *Principles of Plasma Discharges and*  
 621 *Materials Processing* (Second ed.). New York, NY: John Wiley & Sons, Inc.
- 622 Lipschutz, S., Spiegel, M., & Liu, J. (2018). *Schaum's Outline of Mathematical*  
 623 *Handbook of Formulas and Tables* (5th ed.). McGraw-Hill Ed. Retrieved  
 624 from [https://www.ebook.de/de/product/29116254/seymour\\_lipschutz](https://www.ebook.de/de/product/29116254/seymour_lipschutz_murray_spiegel_john_liu_schaum_s_outline_of_mathematical_handbook_of_formulas_and_tables_fifth_edition.html)  
 625 [\\_murray\\_spiegel\\_john\\_liu\\_schaum\\_s\\_outline\\_of\\_mathematical\\_handbook\\_of](https://www.ebook.de/de/product/29116254/seymour_lipschutz_murray_spiegel_john_liu_schaum_s_outline_of_mathematical_handbook_of_formulas_and_tables_fifth_edition.html)  
 626 [\\_formulas\\_and\\_tables\\_fifth\\_edition.html](https://www.ebook.de/de/product/29116254/seymour_lipschutz_murray_spiegel_john_liu_schaum_s_outline_of_mathematical_handbook_of_formulas_and_tables_fifth_edition.html)
- 627 Lorenz, R. D., & Zimelman, J. R. (2014). Venus dunes. In *Dune worlds* (pp. 169–  
 628 176). Springer.
- 629 Lowke, J. J., & D'Alessandro, F. (2003, October). Onset corona fields and electrical  
 630 breakdown criteria. *J. Phys. D: Appl. Phys.*, *36*(21), 2673–2682. doi: 10.1088/  
 631 0022-3727/36/21/013
- 632 Manning, H. L. K., ten Kate, I. L., Battel, S. J., & Mahaffy, P. R. (2010, Novem-  
 633 ber). Electric discharge in the Martian atmosphere, Paschen curves and impli-  
 634 cations for future missions. *Adv. Space Res.*, *46*(10), 1334–1340. doi: 10.1016/  
 635 j.asr.2010.07.006
- 636 Meek, J. M., & Craggs, J. D. (1953). *Electrical Breakdown of Gases* (First ed.). Ox-  
 637 ford, UK: Clarendon Press.
- 638 Melnik, O., & Parrot, M. (1998, December). Electrostatic discharge in Martian dust  
 639 storms. *J. Geophys. Res.*, *103*, 29107–29118. doi: 10.1029/98JA01954

- 640 Méndez Harper, J., Helling, C., & Dufek, J. (2018, November). Triboelectrification of  
641 KCl and ZnS particles in approximated exoplanet environments. *Astrophys. J.*,  
642 *867*(2), 123. doi: 10.3847/1538-4357/aadf36
- 643 Méndez Harper, J. S., McDonald, G. D., Dufek, J., Malaska, M. J., Burr, D. M.,  
644 Hayes, A. G., . . . Wray, J. J. (2017, March). Electrification of sand on Titan  
645 and its influence on sediment transport. *Nat. Geosci.*, *10*(4), 260–265. doi:  
646 10.1038/ngeo2921
- 647 Méndez Harper, J., Dufek, J., & McDonald, G. D. (2021). Detection of spark dis-  
648 charges in an agitated mars dust simulant isolated from foreign surfaces. *Icarus*,  
649 *357*, 114268.
- 650 Méndez Harper, J., Harvey, D., Huang, T., McGrath III, J., Meer, D., & Burton,  
651 J. C. (2022). The lifetime of charged dust in the atmosphere. *PNAS Nexus*,  
652 *1*(5), pgac220.
- 653 Merrison, J., Jensen, J., Kinch, K., Mugford, R., & Nørnberg, P. (2004, March). The  
654 electrical properties of Mars analogue dust. *Planet. Space Sci.*, *52*, 279–290. doi:  
655 10.1016/j.pss.2003.11.003
- 656 Moore, C. B. (1983, January). Improved configurations of lightning rods and air ter-  
657 minals. *J. Franklin Inst.*, *315*(1), 61–85. doi: 10.1016/0016-0032(83)90107-2
- 658 Moore, C. B., Aulich, G. D., & Rison, W. (2000, May). Measurements of lightning  
659 rod responses to nearby strikes. *Geophys. Res. Lett.*, *27*(10), 1487–1490. doi:  
660 10.1029/1999GL011053
- 661 Moore, C. B., Aulich, G. D., & Rison, W. (2003, July). The case for using blunt-  
662 tipped lightning rods as strike receptors. *J. Appl. Meteorol. Climatol.*, *42*(7),  
663 984–993. doi: 10.1175/1520-0450(2003)042<0984:TCFUBL>2.0.CO;2
- 664 Moore, C. B., Rison, W., Mathis, J., & Aulich, G. (2000, May). Lightning rod im-  
665 provement studies. *J. Appl. Meteorol. Climatol.*, *39*(5), 593–609. doi: 10.1175/  
666 1520-0450-39.5.593
- 667 Naidu, M. S., & Kamaraju, V. (2013). *High Voltage Engineering* (Fifth ed.). New York,  
668 NY: McGraw Hill.
- 669 Pancheshnyi, S., Biagi, S., Bordage, M., Hagelaar, G., Morgan, W., Phelps, A., &  
670 Pitchford, L. (2012, apr). The LXCat project: Electron scattering cross sections  
671 and swarm parameters for low temperature plasma modeling. *Chemical Physics*,  
672 *398*, 148–153. doi: 10.1016/j.chemphys.2011.04.020

- 673 Paschen, F. (1889). Über die zum Funkenübergang in Luft, Wasserstoff und  
 674 Kohlensäure bei verschiedenen Drucken erforderliche Potentialdifferenz. *Ann.*  
 675 *Phys.*, *273*(5), 69–96. doi: 10.1002/andp.18892730505
- 676 Pasko, V. P. (2006). Theoretical Modeling of Sprites and Jets. In M. Füllekrug,  
 677 E. A. Mareev, & M. J. Rycroft (Eds.), *Sprites, elves and intense lightning*  
 678 *discharges* (Vol. 225, pp. 253–311). Heidelberg, Germany: Kluwer Academic  
 679 Publishers. doi: 10.1007/1-4020-4629-4\12
- 680 Pitchford, L. C., Alves, L. L., Bartschat, K., Biagi, S. F., Bordage, M.-C., Bray, I.,  
 681 ... Pancheshnyi, S. (2016, September). LXCat: An open-access, web-based  
 682 platform for data needed for modeling low temperature plasmas. *Plasma*  
 683 *Process. Polym.*, *14*(1-2), 1600098. doi: 10.1002/ppap.201600098
- 684 Radebaugh, J., Lorenz, R., Lunine, J., Wall, S., Boubin, G., Reffet, E., ... others  
 685 (2008). Dunes on titan observed by cassini radar. *Icarus*, *194*(2), 690–703.
- 686 Raizer, Y. P. (1991). *Gas Discharge Physics*. New York, NY: Springer-Verlag.
- 687 Rioussset, J. A. (2022, December). "ToTh-1D". Retrieved from [https://github.com/](https://github.com/stroeuim/ToTh-1D)  
 688 [stroeuim/ToTh-1D](https://github.com/stroeuim/ToTh-1D) doi: 10.5281/zenodo.7466017
- 689 Rioussset, J. A., Nag, A., & Palotai, Cs. (2020). Scaling of conventional breakdown  
 690 threshold: Impact for predictions of lightning and TLEs on Earth, Venus, and  
 691 Mars. *Icarus*, *338*, 113506. doi: 10.1016/j.icarus.2019.113506
- 692 Sánchez-Lavega, A., Lebonnois, S., Imamura, T., Read, P., & Luz, D. (2017). The  
 693 atmospheric dynamics of venus. *Space Science Reviews*, *212*(3), 1541–1616.
- 694 Shao, W. D., Zhang, X., Bierson, C. J., & Encrenaz, T. (2020). Revisiting the sulfur-  
 695 water chemical system in the middle atmosphere of venus. *Journal of Geophys-*  
 696 *ical Research: Planets*, *125*(8), e2019JE006195.
- 697 Stumbo, M. T. (2013). *Paschen Breakdown in a CO<sub>2</sub> Atmosphere*. San Luis Obispo,  
 698 CA: Cal. Poly. Retrieved from [http://digitalcommons.calpoly.edu/aerosp/](http://digitalcommons.calpoly.edu/aerosp/114)  
 699 [114](http://digitalcommons.calpoly.edu/aerosp/114) (B.Sc. Thesis)
- 700 Tennakone, K. (2016). Contact electrification of regolith particles and chloride elec-  
 701 trolysis: synthesis of perchlorates on mars. *Astrobiology*, *16*(10), 811–816.
- 702 Thomas, P., & Gierasch, P. J. (1985). Dust devils on mars. *Science*, *230*(4722), 175–  
 703 177.
- 704 Townsend, J. S. (1900, August). The conductivity produced in gases by the motion of  
 705 negatively-charged ions. *Nature*, *62*(1606), 340–341. doi: 10.1038/062340b0

- 706 Townsend, J. S. (1901, February). XVII. The conductivity produced in gases by the  
707 motion of negatively charged ions. *Philos. Mag.*, *1*(2), 198–227. doi: 10.1080/  
708 14786440109462605
- 709 Uman, M. A. (2001). *The Lightning Discharge* (Unabridged ed.). Mineola, NY:  
710 Dover.
- 711 Wurm, G., Schmidt, L., Steinpilz, T., Boden, L., & Teiser, J. (2019, October). A  
712 challenge for martian lightning: Limits of collisional charging at low pressure.  
713 *Icarus*, *331*, 103–109. doi: 10.1016/j.icarus.2019.05.004
- 714 Yair, Y. (2012, August). New results on planetary lightning. *Adv. Space Res.*, *50*(3),  
715 293–310. doi: 10.1016/j.asr.2012.04.013
- 716 Zangwill, A. (2019). *Modern Electrodynamics*. Cambridge Univ. Press.
- 717 Zasova, L., Ignatiev, N., Khatuntsev, I., & Linkin, V. (2007). Structure of the venus  
718 atmosphere. *Planetary and Space Science*, *55*(12), 1712–1728.

1 **A generalized Townsend's theory for Paschen curves in**  
2 **planar, cylindrical, and spherical geometries in**  
3 **planetary atmospheres**

4 **Jeremy A. Rioussset<sup>1,2</sup>, Joshua S. Méndez Harper<sup>3</sup>, Josef Dufek<sup>3</sup>, Jared P.**  
5 **Nelson<sup>2</sup>, Annelisa B. Esparza<sup>2</sup>**

6 <sup>1</sup>Aerospace, Physics & Space Sciences Department, Florida Institute of Technology, 150 W Univ. Blvd.,  
7 Melbourne, FL, 32901, USA

8 <sup>2</sup>Department of Physical Sciences, Space and Atmospheric Instrumentation Lab, Embry-Riddle  
9 Aeronautical University, 1 Aerospace Blvd., Daytona Beach, FL, 32114, USA

10 <sup>3</sup>Department of Earth Sciences, University of Oregon, 1272 University of Oregon, Eugene, OR, 97403,  
11 USA

12 **Key Points:**

- 13 • Numerical modeling lets us study glow coronas around spherical and cylindrical  
14 electrodes based on Paschen theory.
- 15 • Critical voltages are found at  $pd$  and  $pa \approx 0.5 \text{ cm} \cdot \text{Torr}$ , suggesting easier initiation  
16 around mm-size particles in dust and water clouds.
- 17 • Glow corona formation is easier in Mars's low pressure, CO<sub>2</sub>-rich atmosphere than  
18 in Earth's high-pressure atmosphere.

---

Corresponding author: Jeremy A. Rioussset, [riousssej@erau.edu](mailto:riousssej@erau.edu)

19 **Abstract**

20 In this work, we focus on plasma discharges produced between two electrodes with a high  
 21 potential difference, resulting in the ionization of the neutral particles supporting a cur-  
 22 rent in the gaseous medium. At low currents and low temperatures, this process can cre-  
 23 ate luminescent emissions: the glow and corona discharges. The parallel plate geometry  
 24 used in Townsend’s (1900) theory lets us develop a theoretical formalism, with explicit  
 25 solutions for the critical voltage effectively reproducing experimental Paschen curves. How-  
 26 ever, most discharge processes occur in non-parallel plate geometries, such as discharges  
 27 between grains or ice particles in multiphase flows. Here, we propose a generalization  
 28 of the classic parallel plate configurations to concentric spherical and coaxial cylindri-  
 29 cal geometries in Earth, Mars, Titan, and Venus atmospheres. In a spherical case, a small  
 30 radius effectively represents a sharp tip rod, while larger, centimeter-scale radii repre-  
 31 sent blunted tips. Similarly, in a cylindrical case, a small radius corresponds to a thin  
 32 wire. We solve continuity equations in the gap and estimate a critical radius and min-  
 33 imum breakdown voltage that allows ionization of neutral gas and formation of a glow  
 34 discharge. We show that glow coronæ form more easily in Mars’s low-pressure, CO<sub>2</sub>-rich  
 35 atmosphere than in Earth’s high-pressure atmosphere. Additionally, we present break-  
 36 down criteria for Titan and Venus. We further demonstrate that critical voltage minima  
 37 occur at 0.5 cm·Torr for all three investigated geometries, suggesting easier initiation around  
 38 millimeter-size particles in dust and water clouds and could be readily extended to ex-  
 39 amine other multiphase flows with inertial particles.

40 **Plain Language Summary**

41 In this work, we focus on plasma discharges between two electrodes with a high volt-  
 42 age difference. The result is a conversion of the medium from a dielectric to a conduc-  
 43 tor. At low currents and low temperatures, this process can create luminescent emissions:  
 44 the so-called glow and corona discharges. We extend the parallel plate geometry devel-  
 45 oped in Townsend’s (1900) classical theory to determine the critical discharge voltages  
 46 of spheres and cylinders more likely to be encountered as particles in an atmosphere. Here,  
 47 we propose a generalization of the classic parallel plate configurations to concentric spheres  
 48 and coaxial cylinders in Earth, Mars, Venus, and Titan atmospheres. We computation-  
 49 ally solve the continuity equations in the gap between objects and ultimately calculate  
 50 critical electric fields for self-sustained discharges. We show that glow coronæ form more

51 easily in Mars’s low-pressure, CO<sub>2</sub>-rich atmosphere than in Earth’s high-pressure atmo-  
52 sphere. Additionally, we present breakdown criteria for Titan and Venus. We further demon-  
53 strate that critical voltage minima occur near 0.5 cm · Torr for all three investigated ge-  
54 ometries, suggesting easier initiation around millimeter-size particles in dust and water  
55 clouds.

## 56 1 Introduction

57 The recent and planned *in-situ* exploration of planetary bodies in the solar system  
58 motivates a better understanding of electrostatic hazards under conditions relevant to  
59 each object. Specifically, the potential for discharge involves a complex interplay between  
60 atmospheric pressure variation, gas composition, realistic geometries of charged surfaces,  
61 and the presence of suspended solids in the atmosphere. The near-surface, diffuse con-  
62 ditions on present-day Mars may, in particular, present hazards associated with electro-  
63 static discharges for both robotic endeavors and potential crewed missions (Yair, 2012).  
64 Furthermore, the presence (or absence) of electrical discharges could have important im-  
65 plications for atmospheric chemistry and habitability (Tennakone, 2016; Hess et al., 2021).  
66 Any dielectric breakdown starts when the ambient electric field  $E$  exceeds a threshold  
67  $E_{\text{th}}$  (e.g., Raizer, 1991, p. 128), which depends on the nature of the discharge (e.g., leader,  
68 streamer, or glow) and its polarity (see e.g., Pasko, 2006, Figure 1 for discharge in air).  
69 Putative and confirmed extraterrestrial electrical discharges have been the topic of sev-  
70 eral studies (see reviews by Leblanc et al., 2008; Rioussset et al., 2020, and references therein).  
71 While most investigations have focused on lightning as a “transient, high-current elec-  
72 trical discharge whose path length is measured in kilometers” (Uman, 2001, p. 8 & Ta-  
73 ble 14.1), a noteworthy few have also investigated Transient Luminous Events, TLEs (e.g.,  
74 Bering et al., 2004; Dubrovin et al., 2010; Yair, 2012) and small-scale spark or glow dis-  
75 charges (e.g., Méndez Harper et al., 2018; Méndez Harper et al., 2021). Elucidating dis-  
76 charge criteria on extraterrestrial environments is complicated by a profound dearth of  
77 *in-situ* observational data. In the context of Mars, for example, the unfortunate fate of  
78 ExoMars’ Schiaparelli module (Déprez et al., 2014) prevented the first direct measure-  
79 ments of the electric field at the surface of the planet. Insight into the atmospheric elec-  
80 trical environment on Venus and Titan, the two other rocky worlds in our solar systems  
81 with atmospheres thick enough to support gas breakdown, is also scant. Consequently,

82 indirect measurements and analogies remain the only ways to gain insight into breakdown  
83 processes in planetary atmospheres.

84 The diverse span of atmospheric conditions on worlds in our own solar system sug-  
85 gests that the criteria that lead to breakdown in extraterrestrial environments may be  
86 equally disparate. Although both Mars and Venus host CO<sub>2</sub>-rich atmospheres, Venus  
87 maintains a near-surface atmospheric pressure  $\sim 10^4$  times higher than the Martian  
88 one (Zasova et al., 2007; Jakosky, Grebowsky, et al., 2015; Jakosky, Lin, et al., 2015; Sánchez-  
89 Lavega et al., 2017). On Titan, the atmospheric surface pressure is only slightly higher  
90 than Earth’s. However, Titan’s atmosphere is 4 times denser than Earth’s and signifi-  
91 cantly colder (90 K for Titan v. 287 K for Earth (Hörst, 2017)). Important chemical dif-  
92 ferences between worlds exist, too. Methane, for instance, is an important constituent  
93 of Titan’s nitrogen-rich atmosphere. Oxygen, while abundant in Earth’s atmosphere, ex-  
94 ists in trace amounts or is absent in the atmospheres of the other three worlds. Likewise  
95 there is significant variability in the composition, abundance, and presence of particu-  
96 lates in these atmospheres (e.g. silicate dust, ice, hydrocarbons), and multiphase topolo-  
97 gies may also be important for local discharge events. Using this diversity of atmospheric  
98 conditions (summarized in Table 1), we revisit Townsend’s (1900) seminal model for self-  
99 sustained dielectrical breakdown between parallel electrodes. Townsend developed the  
100 theory supporting what is now known as Paschen’s (1889) law. Paschen’s law states that  
101 the breakdown voltage between two electrodes is a function of the product of the pres-  
102 sure,  $p$ , and interelectrode distance,  $d$ . Townsend (1900) proved that this scaling law comes  
103 from the exponential increase of electron number density via avalanche multiplication  
104 and secondary ionization (e.g., Bazelyan & Raizer, 1998, pp. 31–32). Interestingly, these  
105 early studies already involved experiments in air, carbon dioxide, and hydrogen. These  
106 gases contribute significantly to many planetary atmospheres in our solar system, demon-  
107 strating that discharge processes are highly dependent on gas composition.

108 The elegance of Townsend’s theory rests in its simplicity and the sole requirement  
109 of an exponential approximation for the effective ionization coefficient  $\alpha$ . We revisit Townsend’s  
110 theory from first principles in Section 2. Townsend’s theory, however, assumes that the  
111 discharge occurs between two infinite parallel plates (i.e., a 1-D Cartesian geometry). To  
112 approach this configuration, experimental setups have adopted large flat electrodes with  
113 large radii  $R$ , and small gap size,  $d$ , so that  $R \gg d$  (e.g., Raizer (1991, p. 53); Lowke  
114 and D’Alessandro (2003); Stumbo (2013)). While such configurations are suitable for lab-

115 oratory experiments, they may not be representative of real discharge processes that in-  
 116 variably deal with complex geometries. In fact, natural electrical discharge events are  
 117 almost always associated with multiphase flows. For instance, discharges on Mars may  
 118 occur between small sand grains. Similarly, arcing could occur between two voltage-carrying  
 119 conductors under appropriate pressure-distance products. Thus, in the remainder of Sec-  
 120 tion 2, we demonstrate that an extension to cylindrical and spherical geometries is pos-  
 121 sible for Townsend’s theory provided one approximates the mobility  $\mu$ . We further de-  
 122 velop a generalized Townsend’s criterion for the ignition of self-sustained gas discharges

	Earth	Mars	Titan	Venus	
Molar fraction	Ar	$9.05 \times 10^{-3}$	$1.60 \times 10^{-2}$	$2.4 \times 10^{-2}$	–
	CH <sub>4</sub>	–	–	$2.7 \times 10^{-2}$	–
	CO	$1.84 \times 10^{-7}$	–	–	–
	CO <sub>2</sub>	$3.79 \times 10^{-3}$	$95.7 \times 10^{-2}$	–	$96.2 \times 10^{-2}$
	He	$5.04 \times 10^{-6}$	–	–	–
	N <sub>2</sub>	$75.68 \times 10^{-2}$	$2.7 \times 10^{-2}$	$94.9 \times 10^{-2}$	$3.5 \times 10^{-2}$
	N <sub>2</sub> O	$3.43 \times 10^{-7}$	–	–	–
	O <sub>2</sub>	$20.30 \times 10^{-2}$	–	–	–
	O <sub>3</sub>	$3.01 \times 10^{-8}$	–	–	–
$T$ (K)	273.04	231.2	93.9	737	
$N$ (m <sup>-3</sup> )	$2.688 \times 10^{25}$	$1.889 \times 10^{23}$	$1.150 \times 10^{26}$	$9.131 \times 10^{26}$	
Coeff.	$A$ (10 <sup>-20</sup> m <sup>2</sup> )	1.04	2.11	2.14	1.42
	$B$ (Td <sup>-1</sup> )	596.8	594.3	602.5	723.4
	$C$ (10 <sup>24</sup> /(Vms))	3.35	12.32	12.38	3.75
	$D$	-0.23	-0.46	-0.46	-0.23

**Table 1.** Input parameters for BOLSIG runs. Atmospheric parameters are from NASA’s Global Reference Atmospheric Models (GRAMs; EarthGRAM by Leslie (2008), MarsGRAM by H. L. Justh et al. (2010), TitanGRAM by H. Justh and Hoffman (2020), and VenusGRAM by H. L. Justh and Dwyer Cianciolo (2021)) taken at the surface  $z=0$  km on January 1<sup>st</sup>, 2000, 1200 UT, at 0° latitude and 0° longitude. These are the same surface conditions as in (Riousset et al., 2020). The coefficients  $A$ ,  $B$ ,  $C$ , and  $D$  define  $\tilde{a}/N$  and  $\tilde{\mu} \times N$  in (7).

123 for coaxial cylinders and concentric spheres. We show that the numerical solutions of  
 124 these equations yield the critical potential  $V_{cr}$  and corresponding electric field  $E_{cr}$  and  
 125 satisfy the same similarity laws as first introduced by Paschen (1889). Sections 3 and 4  
 126 will respectively discuss the results and implications of the new formalism, while section 5  
 127 will summarize the principal contributions of this paper.

## 128 **2 Model Formulation**

129 This section describes the model used to develop a criterion for the initiation of self-  
 130 sustained glow discharge between two one-dimensional electrodes located at  $r=a$  and  $b$ ,  
 131 where  $r$  is a coordinate along the direction normal to the surface of the electrode (Fig-  
 132 ure 1).

133 In the absence of free electric charges, Gauss's law for electric field  $\vec{E}$  reduces to  
 134  $\nabla \cdot \vec{E} = 0$ . It further simplifies into:

$$135 \frac{1}{r^\delta} \frac{dr^\delta E(r)}{dr} = 0, \quad (1)$$

136 where  $\delta = 0, 1,$  and  $2$  for the Cartesian, cylindrical, spherical 1-D geometries displayed  
 137 in Figures 1a, 1b, and 1c, respectively. If *space charges do not contribute significantly*  
 138 *to the total electric field between the electrodes*, then:  
 139

$$140 E(r) = E_a \left( \frac{a}{r} \right)^\delta, \quad (2)$$

141 with  $E_a = E(a)$  and  $a \leq r \leq b$ .

142 The ignition of an electron avalanche between two electrodes depends on the effec-  
 143 tive ionization frequency  $\nu_i$  and the poorly understood secondary ionization coefficient  
 144  $\gamma$  (Raizer, 1991, p. 74). Townsend's effective ionization coefficient  $\alpha$  provides a conve-  
 145 nient description of the primary ionization per unit length:  
 146

$$147 \alpha = \frac{\nu_i}{\|\vec{u}\|} = \frac{\nu_i}{u} \quad (3)$$

148 where the drift velocity  $\vec{u}$  depends on the mobility  $\mu$  as follows (e.g., Chen, 1984, p. 66):

$$150 \vec{u} = \mu(E) \vec{E}. \quad (4)$$

151 Thus,  $\alpha$  depends on  $E$  as follows:

$$152 \alpha(E) = \frac{\nu_i(E)}{\mu(E)E} \quad (5)$$

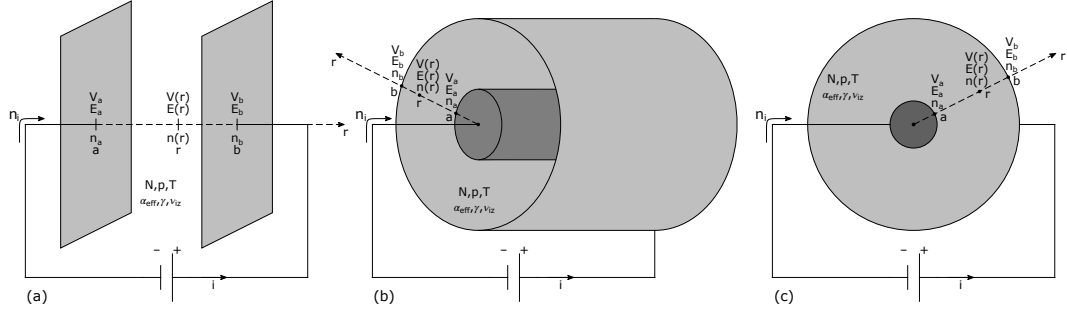


**Figure 1.** Townsend's discharge in one-dimensional geometries: (a) Parallel plates (Cartesian); (b) Coaxial cylindrical electrodes; (c) Concentric spherical electrodes. The gas in between the electrodes has the number density  $N$  ( $\text{m}^{-3}$ ) at the temperature  $T$  (K) under the pressure  $p$  (Pa). The avalanche is characterized by Townsend's effective ionization coefficient  $\alpha$  ( $\text{m}^{-1}$ ), the secondary ionization coefficient  $\gamma$ , and effective ionization frequency  $\nu_i$  ( $\text{s}^{-1}$ ). The quantities  $n_i$ ,  $n_a$ ,  $n(r)$ , and  $n_b$  correspond to the electron density in  $\text{m}^{-3}$  carried by the electronic current  $i$ , emitted from the cathode at  $a$ , measured at  $r$ , and received at the anode at  $b$ , respectively ( $a \leq r \leq b$ ). The corresponding electric potential and field are denoted  $V$  (V) and  $E$  (V/m).

154 Townsend's theory provides an analytical solution to Paschen curves if  $\alpha$  approximately  
 155 fits an exponential function:

$$156 \quad \tilde{\alpha} = Ap \exp(-Bp/E), \quad (6)$$

157  
 158 where  $p$  is the neutral gas pressure (e.g., Raizer, 1991, pp. 149). Experimental studies  
 159 typically adopt pressure-based scaling with  $p$  in Torr and  $\alpha$  in  $\text{cm}^{-1}$  (e.g., Raizer, 1991,  
 160 pp. 133) giving  $\alpha/p$  in  $1/(\text{cm} \cdot \text{Torr})$ . On the other hand, theoretical investigations usu-  
 161 ally prefer density-based scaling with  $N$ , the neutral gas number density in  $\text{m}^{-3}$  and  $\alpha$   
 162 in  $\text{m}^{-1}$ , returning  $\alpha/N$  in  $\text{m}^2$  (e.g., Hagelaar, 2015; Lieberman & Lichtenberg, 2005, p. 545).  
 163 Both formulations are equivalent, provided that the system remains approximately at  
 164 the temperature  $T$  and that the gas obeys the ideal gas law, namely  $p = Nk_B T$ , where  
 165  $k_B$  is the Boltzmann constant. Consequently, we can write:

$$166 \quad \frac{\tilde{\alpha}}{N} = A \exp\left(-\frac{B}{E/N}\right) \quad (7a)$$

$$167 \quad \tilde{\mu} \times N = C \left(\frac{E}{N}\right)^D \quad (7b)$$

168  
 169  
 170

171 where  $A$ ,  $B$ ,  $C$ , and  $D$  are the coefficients from a fit to the reduced Townsend's effective  
 172 ionization  $\alpha/N$  and mobility  $\mu \times N$  (Figure 2) for the atmospheres considered here  
 173 (Table 1).

174 The condition for self-sustainability of Townsend's discharges in any of the geome-  
 175 tries shown in Figure 1 starts with the continuity equation:

$$176 \quad \frac{\partial n}{\partial t} + \nabla \cdot n\vec{u} = n\nu_1 \quad (8)$$

178 where  $n$  is the plasma density.

179 Combining Equations (1), (3), and (8) in a steady state ( $\partial/\partial t = 0$ ) yields  $\frac{1}{r^\delta} \frac{d}{dr} (r^\delta n u) =$   
 180  $n\alpha u$ . Using Equation (4), this simplifies further into:

$$181 \quad \frac{d \ln(r^\delta n \mu(E) E)}{dr} = \alpha(E). \quad (9)$$

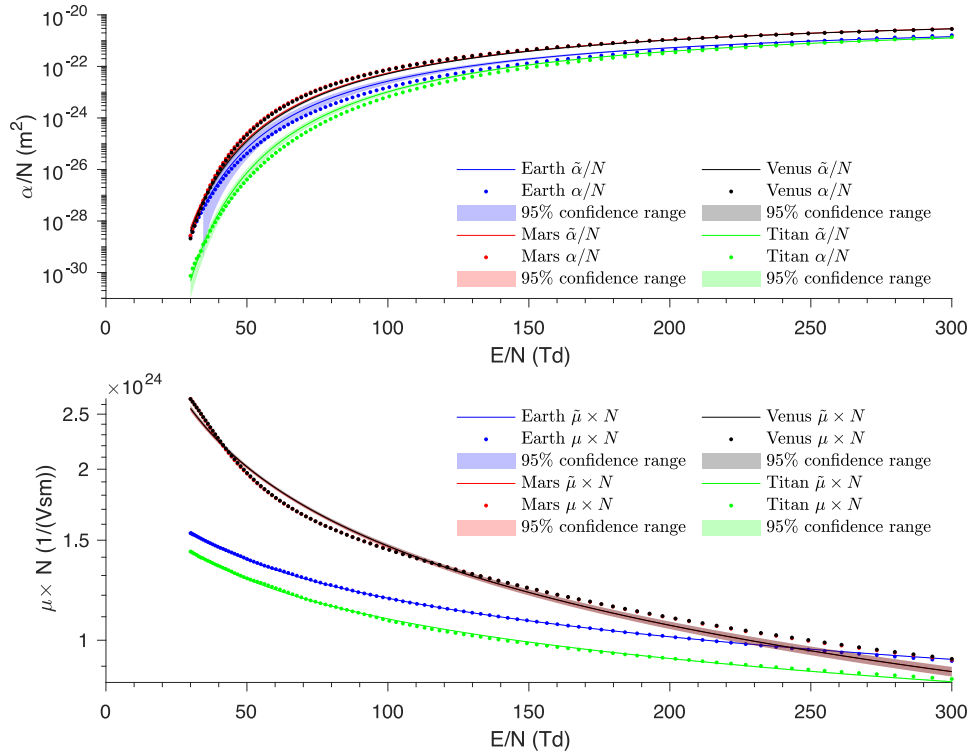


**Figure 2.** Scaling laws for (a) the reduced effective Townsend's ionization coefficient  $\alpha/N$  and (b) reduced mobility  $\mu \times N$  plotted against the reduced electric field  $E/N$ . Blue, red, gray, and green colors correspond to Earth-, Mars-, Venus-, and Titan-like atmospheres, respectively (see Table 1).

183 From Equation (2), we have  $E_a a^\delta = E_b b^\delta$ . If  $A_{\text{av}} = n_b/n_a$  is the avalanche coefficient  
 184 defined as the ratio of the number densities  $n_a = n(a)$  and  $n_b = n(b)$ , then Equa-  
 185 tion (9) yields:

$$186 \quad A_{\text{av}} = \frac{n_b}{n_a} = \frac{\mu(E_a)}{\mu(E_b)} \exp\left(\int_a^b \alpha(E) dr\right) \quad (10)$$

## 188 2.1 Sustainability

189 Call  $n_i$  the number density of charges from the electronic current  $i$  and  $n_\gamma$  the one  
 190 from secondary avalanches between the electrodes, then the conservation of charge pro-  
 191 duces the system below:

$$192 \quad \begin{cases} n_a &= n_i + n_\gamma \\ n_\gamma &= \gamma(n_b - n_a) \cdot \\ n_b &= A_{\text{av}} n_a \end{cases} \quad (11)$$

193 An electron avalanche occurs when the ratio  $n_b/n_i$  diverges (e.g., Naidu & Kamarju, 2013,  
 194 Sec. 2.5). Then, the condition for initiating a self-sustained discharge follows from Equa-  
 195 tion (8):

$$196 \quad \frac{n_b}{n_i} = \frac{A_{\text{av}}}{1 + \frac{1}{\gamma} - A_{\text{av}}} \rightarrow \infty, \quad (12)$$

199 which is satisfied when:

$$200 \quad A_{\text{av}} = 1 + \frac{1}{\gamma}. \quad (13)$$

202 Using Equation (13) to substitute  $A_{\text{av}}$  in Equation (10) yields after simplifications:<sup>1</sup>

$$203 \quad \boxed{\int_a^b \alpha(E) dr + \ln\left(\frac{\mu(E_a)}{\mu(E_b)}\right) = \ln\left(1 + \frac{1}{\gamma}\right)}. \quad (14)$$

205 In all three 1-D cases, Equations (2), (7a), and (7b) let us approximate  $\alpha/N$  and  
 206  $\mu \times N$  as a function of  $a$ ,  $r$ , and  $E_a$ . Thus, the condition of self-sustainability Equa-

---

<sup>1</sup> Note that if  $E_a = E_b$  (e.g., in a parallel plate geometry), one straightforwardly retrieves the classic for-  
 mula (e.g., Raizer, 1991, p. 177).

207 tion (14) in the absence of space charges and displacement field becomes:

$$208 \int_a^b AN \exp\left(-\frac{B}{E_a/N} \left(\frac{r}{a}\right)^\delta\right) dr + D \ln\left(\left(\frac{b}{a}\right)^\delta\right) = \ln\left(1 + \frac{1}{\gamma}\right) \quad (15)$$

209  
210 If  $A$  and  $B$  are converted to  $1/(\text{cm} \cdot \text{Torr})$  and  $V/(\text{cm} \cdot \text{Torr})$  and  $d$  is the distance be-  
211 tween the electrodes ( $b = a + d$ ), then we can show that the scalability of  $E_a/p$  natu-  
212 rally derives from Equation (15) as follows:

$$213 \int_0^d Ap \exp\left(-\frac{B}{E_a/p} \left(1 + \frac{pr}{pa}\right)^\delta\right) dr + D \ln\left(\left(1 + \frac{pd}{pa}\right)^\delta\right) = \ln\left(1 + \frac{1}{\gamma}\right) \quad (16)$$

215 The critical electric field  $E_{\text{cr}}$  is measured at  $r = a$ , therefore  $E_{\text{cr}} = |E_a|$ . Consequently,  
216 Equation (16) yields the following results for the specific geometries described in Figure 1:

$$218 \exp\left(-\frac{Bp}{E_{\text{cr}}}\right) = \frac{1}{Apd} \ln\left(1 + \frac{1}{\gamma}\right) \quad \delta = 0 \quad (17a)$$

$$219 -\frac{E_{\text{cr}}}{Bp} \left[ \exp\left(-\frac{Bp}{E_{\text{cr}}} \left(1 + \frac{pd}{pa}\right)\right) - \exp\left(-\frac{Bp}{E_{\text{cr}}}\right) \right] = \frac{1}{Apa} \ln\left(\frac{\left(1 + \frac{1}{\gamma}\right)}{\left(1 + \frac{pd}{pa}\right)^D}\right) \quad \delta = 1 \quad (17b)$$

$$220 \sqrt{\frac{E_{\text{cr}}}{Bp}} \left[ \text{erf}\left(\sqrt{\frac{E_{\text{cr}}}{Bp}} \left(1 + \frac{pd}{pa}\right)\right) - \text{erf}\left(\sqrt{\frac{E_{\text{cr}}}{Bp}}\right) \right] = \frac{2}{\sqrt{\pi}} \frac{1}{Apa} \ln\left(\frac{\left(1 + \frac{1}{\gamma}\right)}{\left(1 + \frac{pd}{pa}\right)^{2D}}\right) \quad \delta = 2 \quad (17c)$$

222 where  $\text{erf}(x) = \frac{2}{\sqrt{\pi}} \int_0^x e^{-t^2} dt$  is the Gauss error function (e.g., Lipschutz et al., 2018,  
223 p. 203).

## 224 2.2 Critical voltage

225 Paschen curves are plots of the product pressure times density  $pd$  versus critical  
226 electric potential  $V_{\text{cr}}$ . This potential measured between the electrodes at  $a$  and  $b$  ( $V_{\text{cr}} =$   
227  $V_b - V_a$ ) corresponds to the voltage necessary to initiate a self-sustained discharge and  
228 obeys the classic definition  $V(r) = -\int_a^b \vec{E} \cdot d\vec{r}$  (e.g., Zangwill, 2019, p. 62). Equation (2)  
229 then yields  $V_{\text{cr}}$  for the three cases of Figure 1:

$$230 V_{\text{cr}} = E_{\text{cr}}d \quad \delta = 0 \quad (18a)$$

$$231 V_{\text{cr}} = E_{\text{cr}}a \cdot \ln\left(1 + \frac{d}{a}\right) \quad \delta = 1 \quad (18b)$$

$$232 V_{\text{cr}} = E_{\text{cr}}d \cdot \left(1 + \frac{d}{a}\right)^{-1} \quad \delta = 2 \quad (18c)$$

233

For  $\delta = 0$  (case of parallel plates), Equations (17a) and (18a) simplify into the well-established formula (e.g., Raizer, 1991, p. 133):

$$V_{\text{cr}} = \frac{Bpd}{\ln \left( \frac{Apd}{\ln \left( 1 + \frac{1}{\gamma} \right)} \right)} \quad (19)$$

If Equations (17b) and (17c) had known analytical solutions, one could straightforwardly obtain solutions in the cylindrical and spherical geometries ( $\delta=1$  and  $2$ , respectively) from Equations (18b) and (18c). In the absence of closed-form solutions, we use MATLAB `fzero` root-finding algorithm to numerically solve Equation (17) for  $E_{\text{cr}}$  given specific values of  $pa$  and  $pd$ . This function combines the bisection, secant, and inverse quadratic interpolation methods and is based on the works by Brent (1973) and Forsythe et al. (1976). We use the values of  $E_{\text{cr}}$  to deduce the critical voltage  $V_{\text{cr}}$  from Equation (18) given  $pa$ ,  $pd$ , and  $\delta$ .

In the next section, we present the results from our calculation as surface plots for all three geometries of Figure 1 for the environments described in Table 1. We also compare the results to experimental data from the peer-reviewed literature.

### 3 Results

The near-surface atmospheric breakdown criteria for Earth, Mars, Titan, and Venus are summarized in Figures 3 through 6. In each figure, columns (I) and (II) respectively display the critical electric field  $E_{\text{cr}}$  and potential  $V_{\text{cr}}$  for the various geometries explored here as functions  $pd$  and  $pa$ . The results are displayed for values of  $pa$  from  $10^{-1}$  to  $10^{+3}$  cm · Torr and  $pd$  from  $10^{-1}$  to  $10^{+3}$  cm · Torr. The use of pressure-scaled dimensions eases the comparison with experimental data in columns (III) and (IV). Therefore, Figures 3 to 6 use pressure-scaled values ( $E/p$ ,  $pa$ ,  $pd$ ) rather than number-density scaled parameters (e.g.,  $E/N$ ,  $\alpha/N$ ,  $\mu \times N$  in Figure 2). The conversion is possible using the neutral temperatures given in Table 1 and the ideal gas law discussed in Section 2 (see Appendix A for details).

In Figures 3 to 6, the first, second, and third rows display the results for parallel plates, coaxial cylinders, and concentric spherical electrodes, respectively. Specifically, panels (a) and (b) show the calculated values of  $E_{\text{cr}}$  and  $V_{\text{cr}}$  for the parallel plate geometry and confirm that the critical electric field and potential do not vary as a function

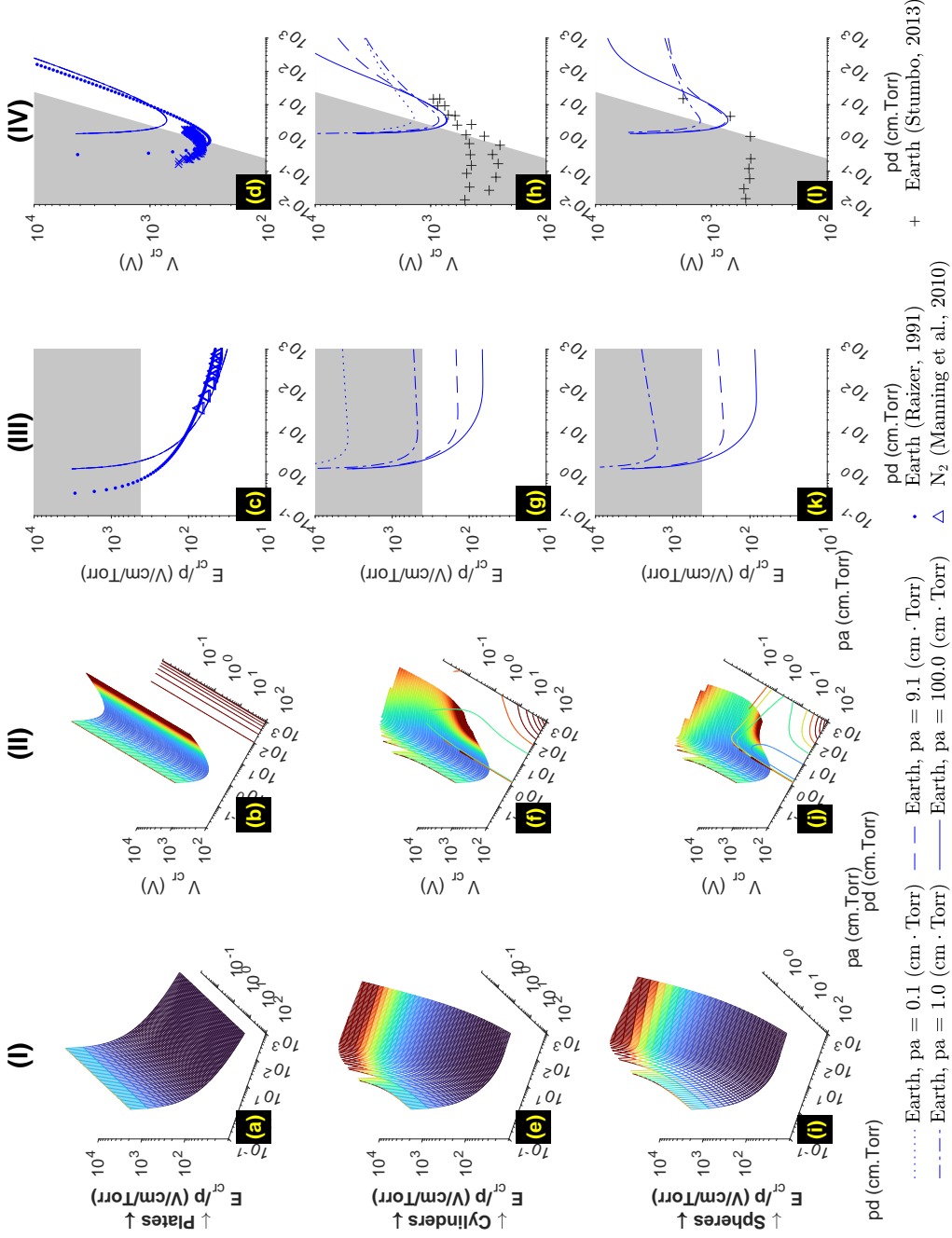


**Figure 3.** Breakdown criteria in the Earth-like atmosphere described in Table 1. The reduced critical electric field  $E_{cr}/p$  is displayed as a function of the reduced size of electrode  $pa$  and distance  $pd$  between electrodes  $a$  and  $b$  in column (I). Column (II) shows  $E_{cr}/p$  vs.  $pd$  for selected  $pa$ -values for comparison with experimental data. Columns (II) and (IV) are the same as columns (I) and (III) but for the critical voltage  $V_{cr}$ . The first, second, and third rows displays the results for electrodes with the following geometries: parallel plates (a-d), coaxial cylinders (e-h), and concentric spheres (i-l). The shaded areas correspond to domains where  $E \geq 10E_k$ .

264 of  $pa$ . Therefore, the surface plots effectively collapse into the well-known curves of Townsend's  
 265 theory. For coaxial cylinders, panels (e) and (f), and concentric spheres, panels (i) and  
 266 (j), Figures 3 to 6 exhibit a similar dependence with  $pd$ , related to the separation between  
 267 the electrodes, but also introduce a new dependence on  $pa$ , emphasizing the role of the  
 268 size of the system for the initiation of self-sustained glow discharge. Conventional Paschen  
 269 curves have a well-defined minimum, Stoletov's point, with a potential  $V_{\min} = \frac{eB}{A} \ln\left(1 + \frac{1}{\gamma}\right)$   
 270 at  $pd_{\min} = \frac{e}{A} \ln\left(1 + \frac{1}{\gamma}\right)$  (e.g., Raizer, 1991, p. 134). However, this minimum point  
 271 becomes a minimum curve in cylindrical and spherical geometries (panels (f) and (j) in  
 272 Figures 3 to 6). As expected, the minimum of the surface plot for the parallel-plate case  
 273 is independent of the value of  $pa$  and obeys Stoletov's equations for  $pd_{\min}$  and  $V_{\min}$ .

274 We compare our numerical results with other numerical calculations and experi-  
 275 mental data in columns (III) and (IV) of Figures 3 to 6. There, we plot selected cross-  
 276 sections from the surface plots in columns (I) and (II). Columns (III) and (IV) display  
 277  $E_{\text{cr}}/p$  and  $V_{\text{cr}}$ , respectively, as a function of the parameter  $pd$  for fixed values of  $pa$ : 0.1,  
 278 1,  $\sim 10$ , and 100 cm·Torr. Experimental measurements in air are rendered in blue mark-  
 279 ers:  $\bullet$  and  $\triangle$  for measurements from (Raizer, 1991) and  $\times$  for Stumbo's (2013) data. Red  
 280 markers display data for Mars:  $\nabla$  for Raizer's (1991) and  $+$  for Manning, ten Kate, Bat-  
 281 tel, and Mahaffy's (2010) works. We further show data for pure CO<sub>2</sub> with black mark-  
 282 ers where  $\bullet$ ,  $\square$ ,  $\nabla$ ,  $+$ ,  $\times$ , and  $\triangleleft$  show the results from (Raizer, 1991), (Hackam, 1969),  
 283 (Buhler et al., 2003), (Manning et al., 2010), (Stumbo, 2013), and (Meek & Craggs, 1953),  
 284 respectively. For comparisons with Earth and Titan scenarios, we included experimen-  
 285 tal results in N<sub>2</sub> from (Manning et al., 2010).

286 As expected, self-sustained discharges between parallel plates do not depend on the  
 287 parameter  $pa$  (see panels (a) and (b) across Figures 3 through 6). Interestingly, Stole-  
 288 tov's points visible in column (IV) occur at similar values of  $pd$  and  $V_{\min}$  ( $\approx 0.1 - 1$  cm · Torr  
 289 and  $\approx 2$  V/cm/Torr, respectively) for the various gas mixtures and geometries. Columns  
 290 (III) and (IV) also show that the theoretical values from Section 2 underestimate experi-  
 291 mental values of  $E_{\text{cr}}$  and  $V_{\text{cr}}$  for all geometries and values of  $pa$ . For a given system, if  
 292 one splits the Paschen curve around the Stoletov's point, one can define a high electric  
 293 field regime for  $pd \ll pd_{\min} \approx 0.1 - 1$  cm · Torr forming the left-hand branch of the  
 294 curves and a high-pressure regime on the right-hand branch of curves for  $pd \gtrsim pd_{\min}$ .

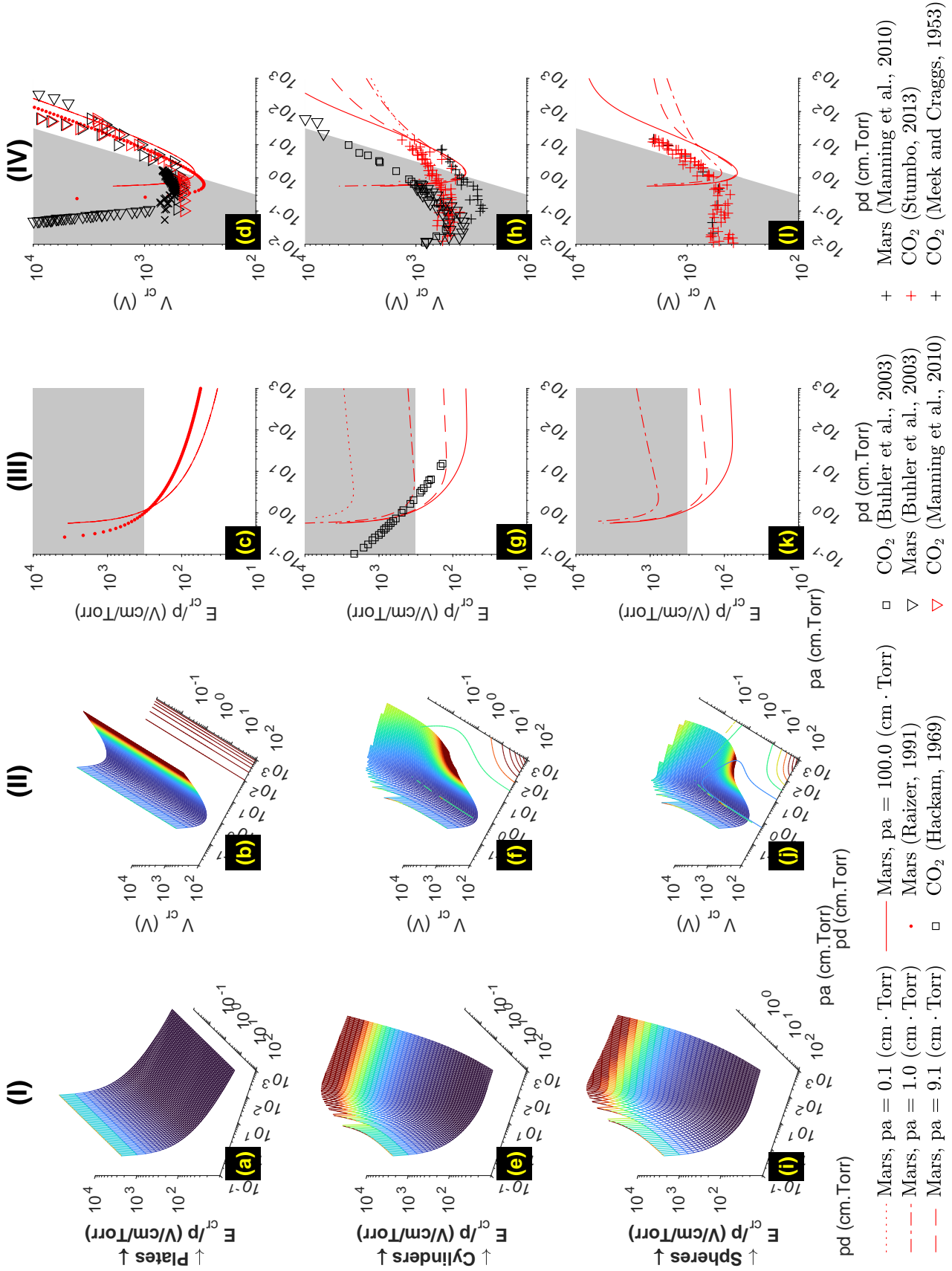


Figure 4. Same as Figure 3 for the Mars-like environment described in Table 1.

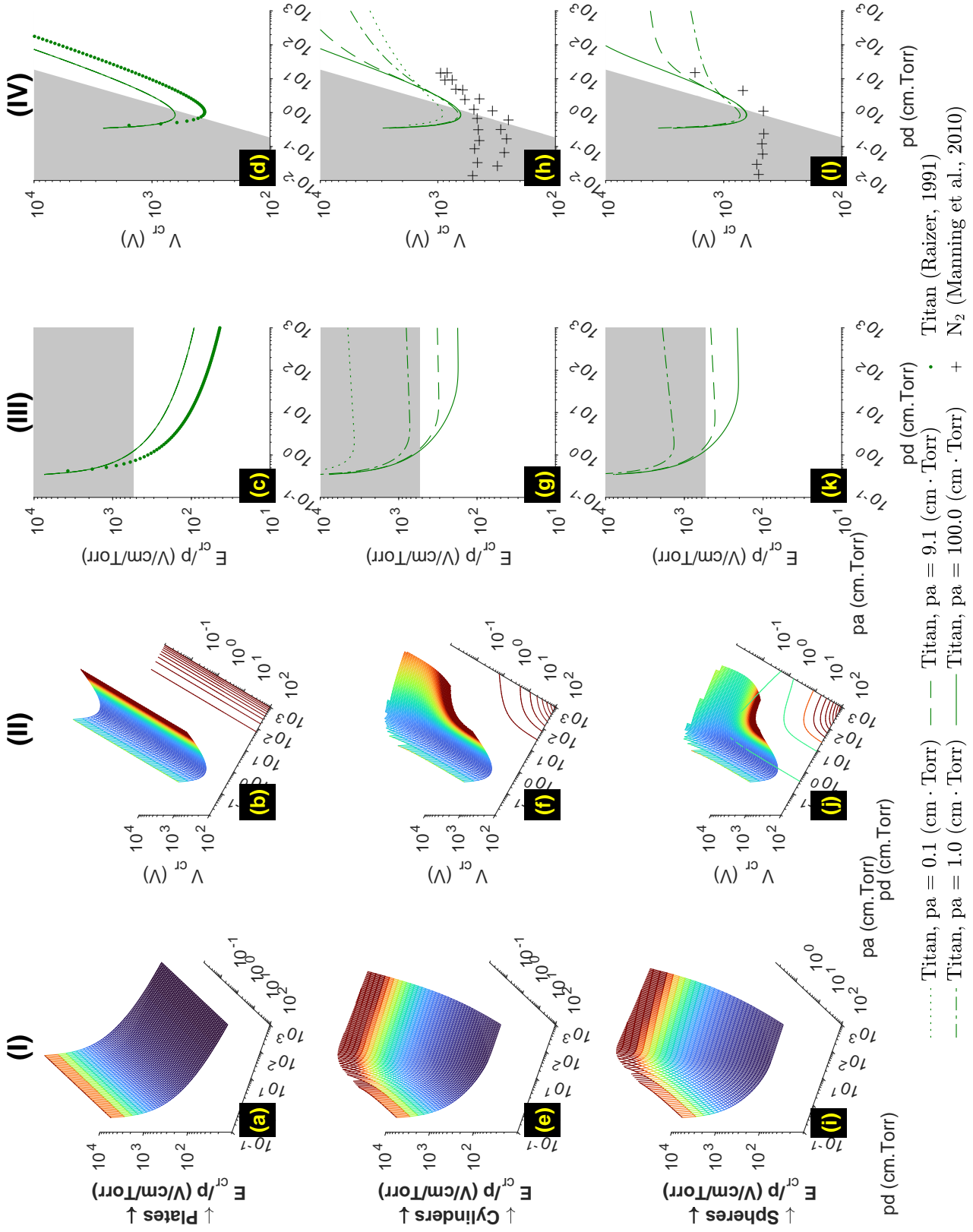


Figure 5. Same as Figure 3 for the Titan-like environment described in Table 1.

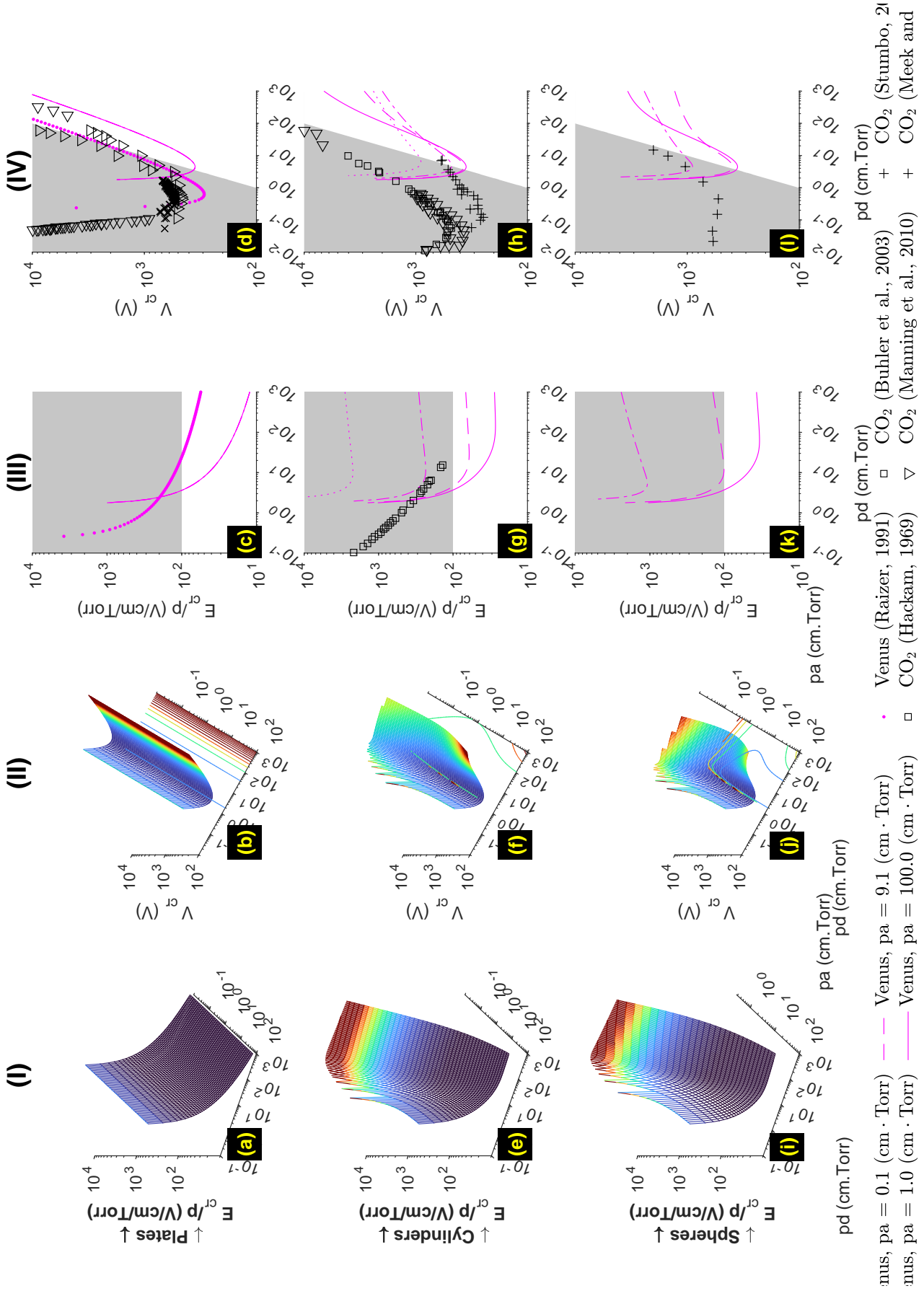


Figure 6. Same as Figure 3 for the Venus-like environment described in Table 1.

295 The right branches of the curves show promising agreement (within an order of mag-  
 296 nitude) between theoretical curves and measurements provided that: (1) one accounts  
 297 for the uncertainty in deriving the coefficients  $A$ ,  $B$ , and  $D$ ; and (2) one carefully con-  
 298 sider the values of  $pa$  best representing the geometries of concentric or coaxial electrodes.  
 299 For these reasons, we shall note that the theoretical slopes closely follow those formed  
 300 by the experimental measurements from various authors (see legends of Figures 3 through  
 301 6 for details). The curves using  $A$  and  $B$  from (Raizer, 1991, p. 56 and ‘•’ markers in  
 302 columns (III) and (IV)) show the influence of these coefficients on the location of Sto-  
 303 letov’s points in theoretical plots. While some authors have derived these values directly  
 304 from the Paschen curves, we derived  $A$ ,  $B$ , and  $D$  from solutions to the Boltzmann equa-  
 305 tion (see Figure 2 and Section 2) to maintain consistency of methodology across coeffi-  
 306 cients and gases. Another explanation of the aforementioned difference stems from the  
 307 differences between pure gases and complex atmospheres (e.g., pure  $\text{CO}_2$  vs. Mars at-  
 308 mospheres, pure  $\text{N}_2$  vs air). Even in cases when the atmospheric composition is almost  
 309 pristine (e.g., Mars’s atmosphere is  $\gtrsim 95\%$   $\text{CO}_2$ ), the presence of minor components  
 310 can dramatically alter the condition for discharge initiation as evidenced by Rioussset et  
 311 al. (2020) in the case of conventional breakdown  $E_k$ .

## 312 4 Discussion

313 The results presented in Section 3 differ from previous attempts at generalizing Townsend’s  
 314 theory of Paschen curves mainly in their full treatment of electron mobility in the con-  
 315 tinuity equation. Neglecting the volume increase along the avalanche path, Raizer (1991,  
 316 p. 177) or Meek and Craggs (1953, p. 100) straightforwardly rewrote the condition for  
 317 initiation of self-sustained discharges Equation (15) as:  $\int_a^b Ap \exp(-Bp/E(r)) dr = \ln(1 + 1/\gamma)$ .  
 318 The proposed formalism here includes the volume change as the electrons move from the  
 319 inner to the outer electrode via the additional mobility term:  $\ln(\mu(E_a)/\mu(E_b)) \approx D \ln((b/a)^\delta)$ .

320 Section 2 has established the equivalence between the classic theory for parallel plate  
 321 electrodes and the equations developed in this work. In addition, the revised equations  
 322 are fully consistent with the well-established scaling laws. We further note that all the  
 323 geometrical parameters in Equation (16) appear in a product with  $p$  (i.e.,  $pa$ ,  $pb$ ,  $pr$ , and  
 324  $pd$ ). Consequently, one must have  $E_{cr} \propto p$  so that Equation (16) remains true if the  
 325 pressure changes with all other parameters remaining the same. Similarly, Equation (18)  
 326 establishes the invariance of the critical voltage  $V_{cr}$  through pressure changes. Writing

327  $E_{\text{cr}} = \frac{E_{\text{cr}}}{p}p$  lets us rewrite Equations (18a), (18b), and (18c) to display the pressure  
 328 scaling explicitly as follows:

$$329 \quad V_{\text{cr}} = \frac{E_{\text{cr}}}{p}pa \cdot \frac{pd}{pa} \quad \delta = 0 \quad (20a)$$

$$330 \quad V_{\text{cr}} = \frac{E_{\text{cr}}}{p}pa \cdot \ln \left( 1 + \frac{pd}{pa} \right) \quad \delta = 1 \quad (20b)$$

$$331 \quad V_{\text{cr}} = \frac{E_{\text{cr}}}{p}pa \cdot \frac{\frac{pd}{pa}}{1 + \frac{pd}{pa}} \quad \delta = 2 \quad (20c)$$

332  
 333 Since  $E_{\text{cr}}/p$  is constant, then  $V_{\text{cr}}$  only depends on the parameters  $pd$  (as in the classic  
 334 Townsend's (1901) theory) and  $pa$ . The previously established scaling law stands with  
 335 the additional parameter  $pa$ . Therefore, Equations (17) and (20) demonstrate that both  
 336 the critical electric field,  $E_{\text{cr}}$ , and potential,  $V_{\text{cr}}$ , are functions of the reduced electrode  
 337 and gap sizes, namely  $pa$  and  $pd$ .

338 Alternately, the ideal gas law,  $p = Nk_{\text{B}}T$ , allows us to rewrite  $E_{\text{cr}}$  and  $V_{\text{cr}}$  as func-  
 339 tions of  $Nd$  and  $Na$ , where  $N$  is the number gas density. This result holds for constant  
 340 gas temperature, which is a reasonable assumption for a cold, non-thermalized discharge  
 341 such as corona or glow. However, it is worth noting that the coefficients  $A$ ,  $B$ , and  $D$   
 342 are derived from a fit to the Boltzmann equation using the parameters given in Table 1.  
 343 The BOLSIG+ solver (Hagelaar, 2015) requires a temperature input while it outputs re-  
 344 duced values for  $\alpha$  and  $\mu$  using the number density  $N$ . The pressure conversion is nec-  
 345 essary to compare to experimental data. The temperatures we used for the four worlds  
 346 are summarized in Table 1. The conversions of the coefficients from density to pressure  
 347 call for the neutral gas temperature (see Appendix A) and this information is required  
 348 for direct comparison between experimental and theoretical Paschen curves. Any mod-  
 349 ification to the  $A$  and  $B$  coefficients will primarily shift the curves and surfaces along  
 350 the vertical  $V_{\text{cr}}$  and horizontal  $pd$  axes of Figures 3 to 6, respectively.

351 In all considered cases,  $E_{\text{cr}}/p$  and  $V_{\text{cr}}$  present an asymptotic behavior towards in-  
 352 finite electric field and potential for low values of  $pd$ , independently of  $pa$ . The values  
 353 on the left branches of the Paschen curves ( $pd \lesssim pd_{\text{min}}$  in column (IV) of Figures 3  
 354 through 6) should be taken with caution as they may not describe the physical mech-  
 355 anism occurring in high-electric fields. Discharges at very low  $pd$  correspond to dielec-  
 356 tric breakdown in a quasi-vacuum. Indeed, Raizer (1991, p. 135) noticed that the electron-  
 357 avalanche process responsible for self-sustained discharges between parallel plates is re-

358 placed by cathode emission at  $pd \lesssim 10^{-3} \text{ cm} \cdot \text{Torr}$ . Thus, the properties of the dis-  
 359 charge are no longer defined by the neutral gas between the electrode, but rather by the  
 360 metallic composition of the electrode. For this reason, the numerical solutions presented  
 361 in this work do not apply in such regimes. On the other hand, the convergence across  
 362 gas compositions at high  $pd$  indicates that the number density of the neutral gas can be-  
 363 come a dominant factor over the molecular electric properties for large gaps under sig-  
 364 nificant pressure. The right branches show similarities to each other across the geome-  
 365 tries at large  $pd \lesssim 100 \text{ cm} \cdot \text{Torr}$ . We advance that these similarities (observed in col-  
 366 umn (IV) of Figures 3 through 6) reflect a regime where the electrode radii of curvature  
 367 are large enough relative to the gap sizes to result in quasi-plane-to-plane conditions.

368 Considering the uncertainty of the electrode geometries in experimental data, the  
 369 theoretical curves are consistent with the measurements. Both approaches indicate min-  
 370 ima in the critical voltages around  $0.5 \text{ cm} \cdot \text{Torr}$ . A simple division by the atmospheric  
 371 pressure returns the gap size most susceptible to trigger a self-sustained discharge in a  
 372 given atmosphere. For example, under a pressure of 760 Torr (Earth’s surface pressure),  
 373 dielectric breakdown may occur in gaps sizes  $\approx 5 \mu\text{m}$  at  $V_{\text{cr}} \lesssim 500 \text{ V}$ . At tropopause’s  
 374 levels,  $p \approx 200 \text{ Torr}$  and the same voltage can initiate a Townsend discharge in a larger  
 375 gap ( $d \approx 25 \mu\text{m}$ ). Similarly, the lower pressure in the Martian atmosphere indicates  
 376 that larger gaps are more prone to dielectric breakdown at the surface of Mars.

377 Panels (f) and (j), i.e., Column (II), of Figures 3 to 6 emphasize the added role of  
 378 mobility in non-planar geometries. In particular, these plots suggest that a reduced ra-  
 379 dius  $pa$  of  $\approx 1 \text{ cm} \cdot \text{Torr}$  is better for initiating self-sustained glow discharges. This cor-  
 380 responds to radii of curvatures  $a \approx 0.05/1 \text{ mm}$  for Earth and  $0.2/5 \text{ mm}$  for Mars at  
 381 ground and cloud levels ( $z \approx 10/20 \text{ km}$ ) in the atmosphere. Such radii of curvature  
 382 are consistent with previous theories that sharp-tipped rods should facilitate the initi-  
 383 ation of upward-connecting leaders and result in better lightning protection, a predic-  
 384 tion contrary to field studies (e.g., Moore, 1983; Moore, Aulich, & Rison, 2000; Moore,  
 385 Rison, et al., 2000; Moore et al., 2003). The paradox therefore remains. However, for Earth,  
 386 the previous calculations indicate that millimeter-sized ice graupels are in the ideal size  
 387 range for discharge initiation at cloud altitude. Beyond meteorological multiphase flows,  
 388 numerous Earth systems transport particles in these size ranges and involve discharges  
 389 processes across a wide range of scales (Crozier, 1964; Kamra, 1972; W. M. Farrell et al.,  
 390 2004; Cimarelli et al., 2022; Méndez Harper et al., 2022). Such flows include gravity cur-

391 rents (dust storms, pyroclastic density currents), volcanic eruption plumes, and wildfire  
392 smoke clouds. Particles in these contexts may have substantial inertia and granular tem-  
393 peratures such that transient optimal gap distances between particles should be common  
394 even in very dilute flows (Dufek et al., 2012; Dufek & Bergantz, 2007). Lastly, if corona  
395 discharge is indeed a precursor to connecting leaders, they can be involved in the pro-  
396 cess of initiation of lightning and Transient Luminous Events (TLEs), jets and sprites  
397 in particular.

398 While this study provides a framework to constrain the capacity of charged surfaces  
399 to cause a breakdown on Mars, Titan, and Venus, how surfaces become electrified on these  
400 worlds remains an area of active research. Mars, for instance, lacks a hydrological cycle  
401 to drive meteorological electrical activity analogous to that on Earth. While Titan and  
402 Venus do have “hydrological” processes that involve the cycle of hydrocarbons and sul-  
403 fur compounds, respectively, whether or not clouds of these compositions are propitious  
404 for discharges remains unknown (Hayes et al., 2018; Shao et al., 2020).

405 However, as is the case for Earth, the three other worlds considered here do host  
406 granular reservoirs that could provide pathways for non-meteorological discharges (Thomas  
407 & Gierasch, 1985; Balme & Greeley, 2006; Radebaugh et al., 2008; Lorenz & Zimbelman,  
408 2014). Martian dust storms involve the movement of large amounts of silicate particles  
409 which invariably undergo collisions. These interactions could charge dust particles via  
410 frictional and contact electrification—collectively known as *triboelectrification* (Horányi  
411 & Lawrence, 2001; Melnik & Parrot, 1998; Merrison et al., 2004; Delory & Farrell, 2011).  
412 Indeed, a broad range of experimental efforts suggests that tribocharging may be quite  
413 efficient within Martian dust events (e.g., Eden & Vonnegut, 1973; Krauss et al., 2003;  
414 Wurm et al., 2019; Méndez Harper et al., 2021). While these experiments have investi-  
415 gated electrification at the grain scale, computer simulations (sometimes combined with  
416 experiments (e.g., Harrison et al., 2016)) have provided useful full-scale expedients for  
417 studies of dust devil electrification (e.g., Melnik & Parrot, 1998; W. M. Farrell et al., 2003).  
418 The results of these studies all converge to the conclusion that electrification in Martian  
419 dust storms should suffice to produce gas breakdown and an atmospheric electric circuit  
420 (W. M. Farrell & Desch, 2001).

421 Similar charging processes may operate on Titan and Venus (or any other world  
422 with mobile granular materials). On Titan, triboelectrification has been associated with

423 the transport of wind-blown hydrocarbon sand (Méndez Harper et al., 2017) and the ag-  
 424 gregation of fine photochemical hazes. Very little work has explored triboelectrification  
 425 under relevant Venusian conditions. However, the presence of dunes and volcanic features  
 426 on Venus indicates particles may charge frictionally during aeolian transport and erup-  
 427 tions (James et al., 2008).

428 Determining the conditions under which atmospheric discharges occur has impli-  
 429 cations for atmospheric chemistry and habitability. Furthermore, discharges could present  
 430 risks to landers and rovers or cause artifacts that confound the interpretation of sensor  
 431 data (Krauss et al., 2003). Recently, for instance, calculations performed by W. Farrell  
 432 et al. (2021) suggest that the rotors of the Ingenuity helicopter could cause localized break-  
 433 down during landing or takeoff. While videography of initial flights has not revealed vi-  
 434 sual evidence for discharges, such events may be best detected electronically. Unfortu-  
 435 nately, Ingenuity does not have the instrumentation to make such measurements. The  
 436 upcoming Dragonfly rotorcraft mission to Titan, however, will involve an electric field  
 437 measurement system (EFIELD) in its DraGMet suite. The main objective of the EFIELD  
 438 experiments is to measure Schumann resonances, which, if detected, would provide ev-  
 439 idence for lightning. Beyond ELF modes, Chatain et al. (2022) have made a compelling  
 440 case that the sensor could be used to detect the movement of charged hydrocarbon sand  
 441 flying past or impinging on the probe during “brownout” conditions. Because (by def-  
 442 inition) discharges also involve the movement of charge, the EFIELD instrument could,  
 443 in principle, detect small-scale breakdown in the vicinity of the rotorcraft. In the case of  
 444 Venus, near-term investigations of discharges in the Venusian environment will remain  
 445 limited to remote sensing observations and analog experiments.

## 446 5 Conclusions

447 The principal results and contributions from this work can be summarized as fol-  
 448 lows:

- 449 1. The theoretical treatment of self-sustained discharge between coaxial cylinders or  
 450 concentric spheres requires a model of mobility. The reduced electron mobility in  
 451 telluric world atmospheres approximately follows a power law:  $\tilde{\mu} \times N = C(E/N)^D$ ,  
 452 where  $C$  and  $D$  are gas-specific constants derived from a numerical fit to the curve  
 453  $E/N$  vs.  $\mu \times N$ .

- 454 2. The newly proposed formalism explains the slope of the Paschen curves in non-  
 455 planar geometries and maintains the scaling laws established by the classic the-  
 456 ory.
- 457 3. In cylindrical and spherical cases, both electrode and gap sizes define the condi-  
 458 tion of discharge initiation. Thus, Paschen curves and Stoletov's points become  
 459 surfaces and curves, respectively.
- 460 4. Critical voltages occur at  $pd$  and  $pa \approx 0.5 \text{ cm} \cdot \text{Torr}$ , suggesting easier initiation around  
 461 millimeter-size particles in dust and water clouds.
- 462 5. Glow corona formation is easier in Mars low pressure,  $\text{CO}_2$ -rich atmosphere than  
 463 in Earth's high-pressure atmosphere.

464 The specific values of the fit coefficients need revising based on laboratory exper-  
 465 iments rather than numerical experiments (i.e., solution of the Boltzmann equation) and  
 466 will be addressed in future work.

## 467 **Appendix A Density vs. pressure scaling**

468 Experimental work typically adopts pressure-scaled variable,  $E/p$ ,  $\alpha/p$ ,  $\mu \times p$  (e.g.,  
 469 columns (III) and (IV) in Figures 3 to 6), while numerical solvers conventionally prefer  
 470 the number density  $N$  as the scaling factor. Calculations of the fit coefficients  $A$ ,  $B$ ,  $C$ ,  
 471 and  $D$  are performed using numerical solutions but require conversion for comparison  
 472 with the peer-reviewed experimental data. Equations (A1) to (A3) provide the conver-  
 473 sion factors.

$$474 \quad \frac{\alpha}{p} = \left( \frac{101325}{100 \cdot 760} \cdot \frac{1}{k_B T} \right) \frac{\alpha}{N} \quad (\text{A1})$$

$$475 \quad \mu \times p = \left( \frac{10^4 \times 760}{101325} \cdot k_B T \right) \mu \times N \quad (\text{A2})$$

$$476 \quad \frac{E}{p} = \left( \frac{101325 \cdot 10^{-21}}{100 \cdot 760} \cdot \frac{1}{k_B T} \right) \frac{E}{N} \quad (\text{A3})$$

478 where the variables have the units indicated in parentheses:  $\alpha/p$  ( $1/(\text{cm} \cdot \text{Torr})$ ),  $\mu \times$   
 479  $p$  ( $(\text{cm}^2 \cdot \text{Torr}) / (\text{V} \cdot \text{s})$ ),  $E/p$  ( $\text{V}/(\text{cm} \cdot \text{Torr})$ ),  $\alpha/N$  ( $\text{m}^2$ ),  $\mu \times N$  ( $1/(\text{V} \cdot \text{m} \cdot \text{s})$ ),  $E/N$  ( $\text{Td}$ ),  
 480  $k_B$  ( $\text{J}/\text{K}$ ), and  $T$  ( $\text{K}$ ), respectively.

481 Similarly, the fit coefficients  $A$  and  $B$  need converting. If indices  $p$  and  $N$  indicate  
 482 the variables used for density and pressure calculations, then:

$$483 \quad A_p = \left( \frac{101325}{100 \cdot 760} \cdot \frac{1}{k_B T} \right) A_N \quad (\text{A4})$$

$$484 \quad B_p = \left( \frac{101325 \cdot 10^{-21}}{100 \cdot 760} \cdot \frac{1}{k_B T} \right) B_N \quad (\text{A5})$$

486 The coefficient  $D$  is unchanged, while  $C$  cancels out from the equations and requires no  
 487 conversion.

## 488 Acknowledgment

489 This work was supported by the National Science Foundation (grant number: 2047863).  
 490 The authors also acknowledge Embry-Riddle Aeronautical University Office of Under-  
 491 graduate Research for supporting Mr. Jacob A. Engle initial contribution to this work.

## 492 Open Research Statement

493 Software for this research is available in these in-text data citation references: (Riousset,  
 494 2022, v1.0.2) under GNU General Public License Version 3, 29 June 2007. Boltzmann's  
 495 equation solver, namely BOLSIG+ is fully described in (Pancheshnyi et al., 2012; Pitch-  
 496 ford et al., 2016; Carbone et al., 2021).

497 The cross-section data used for solving Boltzmann's equation in the study are ob-  
 498 tained from:

- 499 • Hayashi database, [www.lxcat.net](http://www.lxcat.net), retrieved on May 24, 2019.
- 500 • Morgan database, [www.lxcat.net](http://www.lxcat.net), retrieved on May 24, 2019.

501 and available from (Riousset, 2022, v1.0.2).

## 502 CRediT

503 **Jérémy A Riousset:** Conceptualization, Methodology, Software, Formal Anal-  
 504 ysis, Investigation, Resources, Data Curation, Writing - Original draft preparation, Vi-  
 505 sualization, Supervision, Project Administration, Funding Acquisition **Joshua S. Méndes-**  
 506 **Harper:** Validation, Formal Analysis, Investigation, Writing - Original draft prepara-  
 507 tion, Visualization, Funding Acquisition **Josef Dufek:** Validation, Formal Analysis, In-  
 508 vestigation, Resources, Writing - Original draft preparation, Supervision, Project Admin-

509 istration, Funding Acquisition **Jared P. Nelson**: Validation, Formal Analysis, Inves-  
 510 tigation, Writing - Review & Editing **Annelisa B. Esparza**: Investigation, Data Cu-  
 511 ration, Writing - Review & Editing.

## 512 **References**

- 513 Balme, M., & Greeley, R. (2006). Dust devils on Earth and Mars. *Rev. Geophys.*,  
 514 *44*(3). doi: 10.1029/2005rg000188
- 515 Bazelyan, E. M., & Raizer, Y. P. (1998). *Spark Discharge*. New York, NY: Chemical  
 516 Rubber Company Press.
- 517 Bering, E. A., Benbrook, J. R., Bhusal, L., Garrett, J. A., Paredes, A. M., Wescott,  
 518 E. M., . . . Lyons, W. A. (2004). Observations of transient luminous events  
 519 (TLEs) associated with negative cloud to ground (-CG) lightning strokes.  
 520 *Geophys. Res. Lett.*, *31*(5). (L05104) doi: 10.1029/2003GL018659
- 521 Brent, R. P. (1973). *Algorithms for Minimisation without Derivatives*. Englewood  
 522 Cliffs, NJ: Prentice-Hall.
- 523 Buhler, C. R., Calle, C. I., & Nelson, E. (2003, March). Electrical breakdown in a  
 524 Martian gas mixture. In S. Mackwell & E. Stansbery (Eds.), *LPSC* (Vol. 34).  
 525 League City, TX.
- 526 Carbone, E., Graef, W., Hagelaar, G., Boer, D., Hopkins, M. M., Stephens, J. C.,  
 527 . . . Pitchford, L. (2021, February). Data needs for modeling low-temperature  
 528 non-equilibrium plasmas: The LXCat project, history, perspectives and a  
 529 tutorial. *Atoms*, *9*(1), 16. doi: 10.3390/atoms9010016
- 530 Chatain, A., Le Gall, A., Berthelier, J.-J., Lorenz, R. D., Hassen-Khodja, R., Lebre-  
 531 ton, J.-P., . . . Déprez, G. (2022). Detection and characterization of wind-blown  
 532 charged sand grains on titan with the dragmet/efield experiment on dragonfly.  
 533 *Icarus*, 115345.
- 534 Chen, F. F. (1984). *Introduction to Plasma Physics and Controlled Fusion*. New York:  
 535 Plenum Press.
- 536 Cimarelli, C., Behnke, S., Genareau, K., Harper, J. M., & Van Eaton, A. R. (2022).  
 537 Volcanic electrification: recent advances and future perspectives. *Bulletin of Vol-*  
 538 *canology*, *84*(8), 1–10.
- 539 Crozier, W. D. (1964, December). The electric field of a New Mexico dust devil. *J.*  
 540 *Geophys. Res.*, *69*(24), 5427–5429. doi: 10.1029/JZ069i024p05427

- 541 Delory, G., & Farrell, W. (2011). Atmospheric electricity on Mars. In *Epsc-dps joint*  
542 *meeting* (Vol. 6, p. 1229).
- 543 Déprez, G., Montmessin, F., Witasse, O., Lapauw, L., Vivat, F., Abbaki, S., ...  
544 Barth, E. (2014, May). Micro-ARES, an electric-field sensor for ExoMars 2016:  
545 Electric fields modelling, sensitivity evaluations and end-to-end tests. In *Egu*  
546 *general assembly conference abstracts* (Vol. 16, p. 16613).
- 547 Dubrovin, D., Nijdam, S., van Veldhuizen, E. M., Ebert, U., Yair, Y., & Price, C.  
548 (2010, June). Sprite discharges on Venus and Jupiter-like planets: A laboratory  
549 investigation. *J. Geophys. Res.*, *115*(A6). doi: 10.1029/2009ja014851
- 550 Dufek, J., & Bergantz, G. (2007). Suspended load and bed-load transport of particle-  
551 laden gravity currents: the role of particle–bed interaction. *Theoretical and*  
552 *Computational Fluid Dynamics*, *21*(2), 119–145.
- 553 Dufek, J., Manga, M., & Patel, A. (2012). Granular disruption during explosive vol-  
554 canic eruptions. *Nature Geoscience*, *5*(8), 561–564.
- 555 Eden, H. F., & Vonnegut, B. (1973). Electrical breakdown caused by dust motion in  
556 low pressure atmospheres: Considerations for Mars. *Nature*, *280*, 962.
- 557 Farrell, W., McLain, J., Marshall, J., & Wang, A. (2021). Will the mars helicopter  
558 induce local martian atmospheric breakdown? *The Planetary Science Journal*,  
559 *2*(2), 46.
- 560 Farrell, W. M., Delory, G. T., Cummer, S. A., & Marshall, J. R. (2003, October). A  
561 simple electrodynamic model of a dust devil. *Geophys. Res. Lett.*, *30*(20), 2050.  
562 doi: 10.1029/2003GL017606
- 563 Farrell, W. M., & Desch, M. D. (2001, April). Is there a Martian atmospheric electric  
564 circuit? *J. Geophys. Res.*, *106*, 7591–7596. doi: 10.1029/2000JE001271
- 565 Farrell, W. M., Smith, P. H., Delory, G. T., Hillard, G. B., Marshall, J. R., Catling,  
566 D., ... Johnson, B. (2004). Electric and magnetic signatures of dust devils from  
567 the 2000–2001 MATADOR desert tests. *J. Geophys. Res.*, *109*(E3). (E03004)  
568 doi: 10.1029/2003JE002088
- 569 Forsythe, G. E., Malcolm, M. A., & Moler, C. B. (1976). *Computer Methods for Math-*  
570 *ematical Computations*. Englewood Cliffs, NJ: Prentice-Hall.
- 571 Hackam, R. (1969, February). Total secondary ionization coefficients and breakdown  
572 potentials of hydrogen, methane, ethylene, carbon monoxide, nitrogen, oxygen  
573 and carbon dioxide between mild steel coaxial cylinders. *J. Phys. B: At. Mol.*

- 574 *Phys.*, 2(2), 216–233. doi: 10.1088/0022-3700/2/2/309
- 575 Hagelaar, G. J. M. (2015, December). Coulomb collisions in the Boltzmann equa-  
576 tion for electrons in low-temperature gas discharge plasmas. *Plasma Sources Sci.*  
577 *Technol.*, 25(1), 015015. doi: 10.1088/0963-0252/25/1/015015
- 578 Harrison, R. G., Barth, E., Esposito, F., Merrison, J., Montmessin, F., Aplin, K. L.,  
579 ... Zimmerman, M. (2016, April). Applications of electrified dust and dust  
580 devil electrodynamics to Martian atmospheric electricity. *Space Sci. Rev.*,  
581 203(1-4), 299–345. doi: 10.1007/s11214-016-0241-8
- 582 Hayes, A. G., Lorenz, R. D., & Lunine, J. I. (2018). A post-cassini view of titan’s  
583 methane-based hydrologic cycle. *Nature Geoscience*, 11(5), 306–313.
- 584 Hess, B. L., Piazzolo, S., & Harvey, J. (2021). Lightning strikes as a major facilita-  
585 tor of prebiotic phosphorus reduction on early earth. *Nature communications*,  
586 12(1), 1–8.
- 587 Horányi, M., & Lawrence, G. (2001). Charged dust currents on the surface of Mars.  
588 *Phys. Scr.*, 89, 130–132. doi: 10.1238/Physica.Topical.089a00130
- 589 Hörst, S. M. (2017). Titan’s atmosphere and climate. *Journal of Geophysical Re-*  
590 *search: Planets*, 122(3), 432–482.
- 591 Jakosky, B. M., Grebowsky, J. M., Luhmann, J. G., Connerney, J., Eparvier, F., Er-  
592 gun, R., ... Yelle, R. (2015, November). MAVEN observations of the response  
593 of Mars to an interplanetary coronal mass ejection. *Science*, 350, 0210. doi:  
594 10.1126/science.aad0210
- 595 Jakosky, B. M., Lin, R. P., Grebowsky, J. M., Luhmann, J. G., Mitchell, D., Beu-  
596 telschies, G., ... others (2015). The mars atmosphere and volatile evolution  
597 (maven) mission. *Space Science Reviews*, 195(1), 3–48.
- 598 James, M., Wilson, L., Lane, S., Gilbert, J., Mather, T., Harrison, R., & Martin, R.  
599 (2008). Electrical charging of volcanic plumes. *Space Science Reviews*, 137(1),  
600 399–418.
- 601 Justh, H., & Hoffman, J. (2020). Titan global reference atmospheric model (titan-  
602 gram): User guide.
- 603 Justh, H. L., & Dwyer Cianciolo, A. (2021, January). Venus Global Reference At-  
604 mospheric Model (Venus-GRAM) updates. In *43rd COSPAR scientific assem-*  
605 *bly* (Vol. 43, p. 429). Retrieved from [https://ui.adsabs.harvard.edu/abs/](https://ui.adsabs.harvard.edu/abs/2021cosp...43E.429J)  
606 2021cosp...43E.429J (28 January - 4 February)

- 607 Justh, H. L., Justus, C. G., & Badger, A. M. (2010). Updating Mars-GRAM to in-  
 608 crease the accuracy of sensitivity studies at large optical depths. In *COSPAR*  
 609 *Scientific Assembly* (Vol. 38, p. 4).
- 610 Kamra, A. (1972). Physical sciences: Visual observation of electric sparks on gypsum  
 611 dunes. *Nature*, *240*(5377), 143–144.
- 612 Krauss, C. E., Horányi, M., & Robertson, S. (2003, June). Experimental evidence for  
 613 electrostatic discharging of dust near the surface of Mars. *New J. Phys.*, *5*, 70.  
 614 doi: 10.1088/1367-2630/5/1/370
- 615 Leblanc, F., Aplin, K., Yair, Y., Harrison, G., Lebreton, J. P., & Blanc, M. (Eds.).  
 616 (2008). *Planetary Atmospheric Electricity*. New York, NY: Springer-Verlag  
 617 GmbH.
- 618 Leslie, F. (2008). Earth Global Reference Atmospheric Model 2007 (Earth-GRAM07).  
 619 In *COSPAR Scientific Assembly* (Vol. 37, p. 1748).
- 620 Lieberman, M. A., & Lichtenberg, A. J. (2005). *Principles of Plasma Discharges and*  
 621 *Materials Processing* (Second ed.). New York, NY: John Wiley & Sons, Inc.
- 622 Lipschutz, S., Spiegel, M., & Liu, J. (2018). *Schaum's Outline of Mathematical*  
 623 *Handbook of Formulas and Tables* (5th ed.). McGraw-Hill Ed. Retrieved  
 624 from [https://www.ebook.de/de/product/29116254/seymour\\_lipschutz](https://www.ebook.de/de/product/29116254/seymour_lipschutz_murray_spiegel_john_liu_schaum_s_outline_of_mathematical_handbook_of_formulas_and_tables_fifth_edition.html)  
 625 [\\_murray\\_spiegel\\_john\\_liu\\_schaum\\_s\\_outline\\_of\\_mathematical\\_handbook\\_of](https://www.ebook.de/de/product/29116254/seymour_lipschutz_murray_spiegel_john_liu_schaum_s_outline_of_mathematical_handbook_of_formulas_and_tables_fifth_edition.html)  
 626 [\\_formulas\\_and\\_tables\\_fifth\\_edition.html](https://www.ebook.de/de/product/29116254/seymour_lipschutz_murray_spiegel_john_liu_schaum_s_outline_of_mathematical_handbook_of_formulas_and_tables_fifth_edition.html)
- 627 Lorenz, R. D., & Zimbelman, J. R. (2014). Venus dunes. In *Dune worlds* (pp. 169–  
 628 176). Springer.
- 629 Lowke, J. J., & D'Alessandro, F. (2003, October). Onset corona fields and electrical  
 630 breakdown criteria. *J. Phys. D: Appl. Phys.*, *36*(21), 2673–2682. doi: 10.1088/  
 631 0022-3727/36/21/013
- 632 Manning, H. L. K., ten Kate, I. L., Battel, S. J., & Mahaffy, P. R. (2010, Novem-  
 633 ber). Electric discharge in the Martian atmosphere, Paschen curves and impli-  
 634 cations for future missions. *Adv. Space Res.*, *46*(10), 1334–1340. doi: 10.1016/  
 635 j.asr.2010.07.006
- 636 Meek, J. M., & Craggs, J. D. (1953). *Electrical Breakdown of Gases* (First ed.). Ox-  
 637 ford, UK: Clarendon Press.
- 638 Melnik, O., & Parrot, M. (1998, December). Electrostatic discharge in Martian dust  
 639 storms. *J. Geophys. Res.*, *103*, 29107–29118. doi: 10.1029/98JA01954

- 640 Méndez Harper, J., Helling, C., & Dufek, J. (2018, November). Triboelectrification of  
641 KCl and ZnS particles in approximated exoplanet environments. *Astrophys. J.*,  
642 *867*(2), 123. doi: 10.3847/1538-4357/aadf36
- 643 Méndez Harper, J. S., McDonald, G. D., Dufek, J., Malaska, M. J., Burr, D. M.,  
644 Hayes, A. G., . . . Wray, J. J. (2017, March). Electrification of sand on Titan  
645 and its influence on sediment transport. *Nat. Geosci.*, *10*(4), 260–265. doi:  
646 10.1038/ngeo2921
- 647 Méndez Harper, J., Dufek, J., & McDonald, G. D. (2021). Detection of spark dis-  
648 charges in an agitated mars dust simulant isolated from foreign surfaces. *Icarus*,  
649 *357*, 114268.
- 650 Méndez Harper, J., Harvey, D., Huang, T., McGrath III, J., Meer, D., & Burton,  
651 J. C. (2022). The lifetime of charged dust in the atmosphere. *PNAS Nexus*,  
652 *1*(5), pgac220.
- 653 Merrison, J., Jensen, J., Kinch, K., Mugford, R., & Nørnberg, P. (2004, March). The  
654 electrical properties of Mars analogue dust. *Planet. Space Sci.*, *52*, 279–290. doi:  
655 10.1016/j.pss.2003.11.003
- 656 Moore, C. B. (1983, January). Improved configurations of lightning rods and air ter-  
657 minals. *J. Franklin Inst.*, *315*(1), 61–85. doi: 10.1016/0016-0032(83)90107-2
- 658 Moore, C. B., Aulich, G. D., & Rison, W. (2000, May). Measurements of lightning  
659 rod responses to nearby strikes. *Geophys. Res. Lett.*, *27*(10), 1487–1490. doi:  
660 10.1029/1999GL011053
- 661 Moore, C. B., Aulich, G. D., & Rison, W. (2003, July). The case for using blunt-  
662 tipped lightning rods as strike receptors. *J. Appl. Meteorol. Climatol.*, *42*(7),  
663 984–993. doi: 10.1175/1520-0450(2003)042<0984:TCFUBL>2.0.CO;2
- 664 Moore, C. B., Rison, W., Mathis, J., & Aulich, G. (2000, May). Lightning rod im-  
665 provement studies. *J. Appl. Meteorol. Climatol.*, *39*(5), 593–609. doi: 10.1175/  
666 1520-0450-39.5.593
- 667 Naidu, M. S., & Kamaraju, V. (2013). *High Voltage Engineering* (Fifth ed.). New York,  
668 NY: McGraw Hill.
- 669 Pancheshnyi, S., Biagi, S., Bordage, M., Hagelaar, G., Morgan, W., Phelps, A., &  
670 Pitchford, L. (2012, apr). The LXCat project: Electron scattering cross sections  
671 and swarm parameters for low temperature plasma modeling. *Chemical Physics*,  
672 *398*, 148–153. doi: 10.1016/j.chemphys.2011.04.020

- 673 Paschen, F. (1889). Über die zum Funkenübergang in Luft, Wasserstoff und  
674 Kohlensäure bei verschiedenen Drucken erforderliche Potentialdifferenz. *Ann.*  
675 *Phys.*, *273*(5), 69–96. doi: 10.1002/andp.18892730505
- 676 Pasko, V. P. (2006). Theoretical Modeling of Sprites and Jets. In M. Füllekrug,  
677 E. A. Mareev, & M. J. Rycroft (Eds.), *Sprites, elves and intense lightning*  
678 *discharges* (Vol. 225, pp. 253–311). Heidelberg, Germany: Kluwer Academic  
679 Publishers. doi: 10.1007/1-4020-4629-4\12
- 680 Pitchford, L. C., Alves, L. L., Bartschat, K., Biagi, S. F., Bordage, M.-C., Bray, I.,  
681 ... Pancheshnyi, S. (2016, September). LXCat: An open-access, web-based  
682 platform for data needed for modeling low temperature plasmas. *Plasma*  
683 *Process. Polym.*, *14*(1-2), 1600098. doi: 10.1002/ppap.201600098
- 684 Radebaugh, J., Lorenz, R., Lunine, J., Wall, S., Boubin, G., Reffet, E., ... others  
685 (2008). Dunes on titan observed by cassini radar. *Icarus*, *194*(2), 690–703.
- 686 Raizer, Y. P. (1991). *Gas Discharge Physics*. New York, NY: Springer-Verlag.
- 687 Rioussset, J. A. (2022, December). "ToTh-1D". Retrieved from [https://github.com/](https://github.com/stroeuim/ToTh-1D)  
688 [stroeuim/ToTh-1D](https://github.com/stroeuim/ToTh-1D) doi: 10.5281/zenodo.7466017
- 689 Rioussset, J. A., Nag, A., & Palotai, Cs. (2020). Scaling of conventional breakdown  
690 threshold: Impact for predictions of lightning and TLEs on Earth, Venus, and  
691 Mars. *Icarus*, *338*, 113506. doi: 10.1016/j.icarus.2019.113506
- 692 Sánchez-Lavega, A., Lebonnois, S., Imamura, T., Read, P., & Luz, D. (2017). The  
693 atmospheric dynamics of venus. *Space Science Reviews*, *212*(3), 1541–1616.
- 694 Shao, W. D., Zhang, X., Bierson, C. J., & Encrenaz, T. (2020). Revisiting the sulfur-  
695 water chemical system in the middle atmosphere of venus. *Journal of Geophys-*  
696 *ical Research: Planets*, *125*(8), e2019JE006195.
- 697 Stumbo, M. T. (2013). *Paschen Breakdown in a CO<sub>2</sub> Atmosphere*. San Luis Obispo,  
698 CA: Cal. Poly. Retrieved from [http://digitalcommons.calpoly.edu/aerosp/](http://digitalcommons.calpoly.edu/aerosp/114)  
699 [114](http://digitalcommons.calpoly.edu/aerosp/114) (B.Sc. Thesis)
- 700 Tennakone, K. (2016). Contact electrification of regolith particles and chloride elec-  
701 trolysis: synthesis of perchlorates on mars. *Astrobiology*, *16*(10), 811–816.
- 702 Thomas, P., & Gierasch, P. J. (1985). Dust devils on mars. *Science*, *230*(4722), 175–  
703 177.
- 704 Townsend, J. S. (1900, August). The conductivity produced in gases by the motion of  
705 negatively-charged ions. *Nature*, *62*(1606), 340–341. doi: 10.1038/062340b0

- 706 Townsend, J. S. (1901, February). XVII. The conductivity produced in gases by the  
707 motion of negatively charged ions. *Philos. Mag.*, *1*(2), 198–227. doi: 10.1080/  
708 14786440109462605
- 709 Uman, M. A. (2001). *The Lightning Discharge* (Unabridged ed.). Mineola, NY:  
710 Dover.
- 711 Wurm, G., Schmidt, L., Steinpilz, T., Boden, L., & Teiser, J. (2019, October). A  
712 challenge for martian lightning: Limits of collisional charging at low pressure.  
713 *Icarus*, *331*, 103–109. doi: 10.1016/j.icarus.2019.05.004
- 714 Yair, Y. (2012, August). New results on planetary lightning. *Adv. Space Res.*, *50*(3),  
715 293–310. doi: 10.1016/j.asr.2012.04.013
- 716 Zangwill, A. (2019). *Modern Electrodynamics*. Cambridge Univ. Press.
- 717 Zasova, L., Ignatiev, N., Khatuntsev, I., & Linkin, V. (2007). Structure of the venus  
718 atmosphere. *Planetary and Space Science*, *55*(12), 1712–1728.